Optical Measurement of Directional, Regional, and Strain Rate Dependent Mechanical Properties of Human Brain Tissue under Uniaxial Compression

by

Alejandro Matos Camarillo

A thesis submitted in partial fulfillment of the requirements for the degree of

Master of Science

Department of Mechanical Engineering
University of Alberta

Abstract

The brain is the most important central nervous system component, consisting of a complex network of neurons and glial cells essential for information processing, movement, and behavior control. It is encased within the skull and suspended in cerebrospinal fluid (CSF), but its low rigidity makes it susceptible to damage from mechanically induced trauma. It can be differentiated into gray and white matter, respectively composed of neuron cell bodies and myelinated axon fibers. The various regions of the brain contain differing proportions of these tissue types, adding to the overall complexity of the brain's structure. While computational models have helped advance the development of diagnostic tools and the establishment of injury thresholds, there still exist gaps in the understanding of the mechanical properties of human brain tissue under different loading conditions. The brain's heterogeneous structure is believed to influence the variation in mechanical properties reported in biomechanics literature. This complexity challenges the investigation and modeling of brain tissue, which cannot be assumed homogeneous as previously thought. This thesis sought to address gaps in the brain mechanics literature by examining the mechanical behavior of human brain tissue under uniaxial compression loading. The analysis focused on the regional, directional, and strain-rate dependent variations in properties from a continuum mechanics experimental approach utilizing uniaxial compression tests combined with Digital Image Correlation (DIC) to analyze the stress response and the deformation of human brain tissue samples at perpendicular planes of view. Tissues from two distinct brain regions were analyzed: the gray cortical matter of the temporal lobe and white matter from the corpus callosum, each

subjected to various strain rates and magnitudes. In the corpus callosum, loading was applied parallel and perpendicular to the axon fiber orientation to study anisotropy due to the fiber orientation.

Experimental results demonstrated that the stress response of brain tissue increased with both strain rate and magnitude in all examined regions and loading directions. However, comparisons between regions revealed no differences in stress-stretch responses. Utilizing DIC to assess the transverse and axial strains of the samples during mechanical testing revealed that the Poisson's ratio (PR) of the tissues changed with the stretch level, hence termed the Poisson Function (PF). The temporal lobe exhibited isotropic behavior, closely aligning with the behavior of a homogeneous incompressible material. In the corpus callosum, the differing PF behavior across planes of view and loading directions suggested a transversely isotropic response. The volume ratio investigations showed slight deviations from incompressible behavior with both strain rate and magnitude that can result in large stored energy penalties due to the high bulk modulus of brain tissue.

This study addressed existing gaps in human brain tissue behavior at strain rates representative of trauma events in comparison to quasistatic strain rates. A key highlight of this work is the detailed investigation of the corpus callosum, examining its deformation characteristics in relation to its axon fiber orientation. This thesis provided insights into the PF evolution as a function of stretch that helps in understanding the anisotropy of brain tissue. Analyzing the volume ratio evolution provided insight into the compressibility of the tissue that is not attainable by analyzing the PR alone. Altogether, the observations from this thesis highlight the complex mechanics of brain tissue and provide evidence for the anisotropic behavior of white matter, and the importance of considering strain rate, and compressibility in future biomechanical modeling efforts.

Preface

This thesis is an original work by Alejandro Matos Camarillo. No part of this thesis has been previously published.

The research project, of which this thesis is a part, received research ethics approval from the University of Alberta Research Ethics Board, Project Name "Mechanical properties of human brain tissue", ID: Pro00135530, Nov 2, 2023.

Acknowledgements

I want to start by expressing my deepest gratitude to my supervisors, Drs. Dan Romanyk and James Hogan. Your guidance and support have been pivotal in my academic journey. You've not only challenged me but also fostered my professional and personal growth. I can't thank you enough for believing in me and pushing me to explore my full potential.

I would like to thank Dr. Karyne Rabey for her invaluable expertise and collaboration that has been essential to my research, and I genuinely appreciate the role you and Hugh Barrett played in making this project a reality.

To my colleagues at the Romanyk Lab and CDAM, your collaborative spirit and constant encouragement have been invaluable. Working and learning alongside such a talented group has been both an honor and a pleasure.

I would also like to acknowledge the anonymous donors of the anatomical gifts program and their families. Your donation to science is profoundly respected and has been instrumental in our commitment to the advancement of knowledge.

Lastly, I want to thank my friends and family for their unwavering support. I am especially grateful to my wife, Katy, whose countless sacrifices have been a fundamental force in bringing this thesis to fruition.

Table of Contents

List of Tables

List of Figures

List of Symbols

Latin

A	Cross-sectional area
F	Force
J	Volume ratio
K	Bulk modulus
W^{Ogd}	Strain energy function (Ogden)
$W^{\mathrm{Ogd}}_{\mathrm{iso}}$	Isochoric part of strain energy function
$W^{\mathrm{Ogd}}_{\mathrm{vol}}$	Volumetric part of strain energy function

Greek

α	Material parameter relating to tissue stiffness
$\bar{\lambda}_i$	Isochoric principal stretches
λ_i	Stretch ratio
μ	Material parameter relating to shear modulus
σ	Stress
ε	Strain

Abbreviations

CC Corpus Callosum.

CCwF Corpus Callosum compressed along fibers.

CCxF Corpus Callosum compressed across fibers.

CSF Cerebrospinal Fluid.

CT Computed Tomography.

DIC Digital Image Correlation.

ECM Extracellular Matrix.

FE Final Element.

MRI Magnetic Resonance Imaging.

PBS Phosphate Buffered Saline.

PF Poisson Function.

PR Poisson's Ratio.

ROI Region of Interest.

TBI Traumatic Brain Injury.

TL Temporal Lobe.

ZNSSD Zero-Normalized Sum of Squared Differences.

Chapter 1

Introduction

This chapter introduces the importance of investigating the variation in mechanical properties in brain tissue depending on region, direction, strain magnitude, and rate of applied loading. This chapter will also present the thesis objectives, organization, and contributions.

1.1 Thesis Motivation

Head injuries are a significant cause of mortality, prompting intensive research into brain tissue mechanics [1]. These efforts aim to not only save lives by improving clinical diagnoses but also to lessen the suffering that often follows such injuries by reducing the rate of clinical failure [2]. More specifically, studying tissue mechanics can help unravel injury mechanisms, quantify tissue responses, establish injury thresholds, and assist in planning surgical procedures [3]. Traumatic Brain Injuries (TBIs) represent one of the deadliest forms of trauma, primarily due to the brain's remarkable softness, intricate microstructure, complex behavior under external loading, and the common irreversible damage caused by these injuries [3, 4].

Brain tissue is composed of up to 80% water, of which 20-40% is free-flowing cerebrospinal fluid (CSF) that surrounds the brain and provides nourishment and protection [5, 6]. Brain tissue can be categorized into gray and white matter. The gray matter contains neuron cell bodies, while the white matter contains the neuron

axon fibers [7]. This microstructural difference is thought to cause the variations in mechanical properties observed in the literature [3], leading to efforts in characterizing the spatial variations in the mechanical properties of tissue [7–9]. However, differences in experimental protocols for investigating tissue properties have delayed reaching a consensus on the effects of brain structural variation within the scientific community [10].

Several experimental and computational studies based on continuum mechanics approaches have provided important insights into the mechanisms of injury that are otherwise not attainable using diagnostic tools such as Magnetic Resonance Imaging (MRI) or Computed Tomography (CT) [11]. Despite these insights, there are still several gaps in the understanding of the mechanical behavior of brain tissue that must be addressed to more effectively model tissue behavior [12, 13].

Research on the corpus callosum, a dense, uniaxially oriented axon fiber region connecting the brain's hemispheres, has revealed its potential for exploring the influence of axon orientation on mechanical behavior [12–14]. Both animal and human studies have shown evidence of mechanical anisotropy in the brain's white matter under shear [15], indentation [16], tension [17], and compression [18] conditions. When summarizing the literature on white matter anisotropy, it is necessary to account for the deformation rates and magnitudes applied in the experiments, as these factors influence the observed anisotropic characteristics and their interpretation. For instance, one study that conducted shear, compression, and tension mechanical testing on cuboid human brain tissue samples [7], did not observe anisotropy effects in any loading mode when applying a 10% strain and $0.00667s^{-1}$ strain rate. In contrast, another study on human brain tissue performing tests under the same loading modes [9], in this case to 50% strain and strain rates up to $30s^{-1}$ reported anisotropic effects on shear tests only. However, a different study observed anisotropic effects in compression tests conducted on porcine brain tissue [18]. These findings suggest that the manifestation of anisotropy in white matter may be significantly influenced by both

the magnitude and rate of deformation, as well as the specifics of the experimental protocol such as sample dimensions, and species of the brain tissue tested.

Due to its high water content, brain tissue has often been assumed either incompressible or nearly incompressible [13, 17, 19, 20]. Most time-independent constitutive models define the elastic material properties of brain tissue as hyperelastic and incompressible [12]. The incompressibility approximation allows for the simplification of the constitutive equations [21], but the effects of this assumption have not been fully explored. Non-contact strain measurement techniques, such as Digital Image Correlation (DIC), have enabled the measurement of displacements and strains on the surfaces of delicate tissue samples during mechanical tests [22]. This technique is useful in the assessment of brain tissue compressibility, particularly in the analysis of Poisson's Ratio (PR) and volume ratio [14, 23, 24].

In the literature, the experimental investigations of brain tissue compressibility are scarce and have focused on measuring the PR of white matter from the corona radiata and brain stem [14, 24], and of mixed gray-white matter tissue [14] at specific strain magnitudes. Another study measured the volume ratio of mixed gray and white tissue under the assumption of homogeneous and isotropic behavior [23]. Using animal tissues, all studies concluded that brain tissue can be assumed as incompressible at strains of up to 10% [14, 23, 24]. It is said in these studies that for tissue to be incompressible, the PR of the tissue should be equal to or close to 0.5. Yet, regardless of the degree of incompressibility of a material, at large deformations, the PR becomes a function of axial strain [25]. Additionally, the mechanical response of anisotropic materials can vary depending on the direction of the applied stress and the PR values are not bound by $-1 \leq PR \leq 0.5$ as is the case for isotropic materials [26]. Thus, the PR may not be suitable for assessing tissue compressibility in all scenarios, given the ongoing debate about potential anisotropy within the white matter due to the axon fiber orientation [3, 10, 12, 16].

Understanding the compressibility behavior of brain tissue under small strains is

important for cases such as minimizing unintended tissue damage during neurosurgical operations [27]. However, traumatic events often cause strains within the brain exceeding 20% [28], highlighting the importance of investigating the large strain compressibility behavior that is currently missing from the literature. Experimental challenges, such as the need for small sample sizes when testing isolated tissue types (e.g., gray cortical matter, white matter from the corpus callosum [7, 14]), the requirement of sample surface preparation for optical strain measurement [14], and the scarcity of human brain tissue for research, complicate the study of brain tissue compressibility and its variation with regional, directional, and load rate and magnitude changes [14]. Consequently, there is a gap in the literature regarding the investigation of human brain tissue compressibility, focusing on a range of deformation rates and magnitudes reflective of those observed in TBI cases.

1.2 Thesis Objectives

The objective of this thesis was to advance the understanding of regional variation in the stress-stretch behavior of human brain tissue and to provide experimental evidence to assess the validity of the incompressibility assumption in the mathematical modeling of brain tissue across regions, strain rates, strain magnitudes, and loading directions. For this, an investigation of the isotropy and compressibility of the brain tissue was conducted by measuring and analyzing the evolution of the PR and volume ratio as a function of axial stretch. This involved adopting a continuum approach to analyze brain tissue at the macroscopic scale using mechanical testing combined with DIC analysis. Non-contact measurement of axial and lateral strains of brain tissue samples in two different planes of view for deformations up to 0.7 stretch (or 30% strain). The goal of this thesis was achieved by conducting uniaxial compression experiments on human gray and white matter tissues at $0.05/s$ and $5/s$ strain rates. For the white matter tissue tests, the effect of varying loading direction relative to the tissue's fiber orientation was also investigated.

This thesis specifically draws tissues from 2 regions in the brain:

1. Gray cortical matter from the temporal lobe, consists of neuron cell bodies [7], and is largely considered isotropic. The temporal lobe is a relevant region to study due to its common involvement in TBI events [29].

2. White matter from the corpus callosum, a region that provides communication between the two brain hemispheres, and is largely composed of uniaxially oriented axon fibers [7]. The anisotropy of this region and the effect of the fiber direction is not well established in the literature [13]

1.3 Thesis Organization

This thesis is comprised of four chapters. Chapter 2 provides an overview of human brain anatomy and physiology, discusses previously used testing protocols for studying brain tissue's mechanical properties, and summarizes prior research on brain tissue compression that utilized the DIC analysis method to investigate its compressibility. Chapter 3 details the experimental design and its execution for assessing the stress-stretch relationship, and the evolution of PR and volume ratio in the temporal lobe and corpus callosum tissues as a function of axial stretch and loading rate. Chapter 4 provides a comprehensive discussion of the contributions and conclusions drawn from this thesis. It also explores the potential applications of the findings and methods presented within this work and outlines the limitations associated with the research. Appendix A contains supplemental content regarding DIC, including a summary of the method, sample preparation procedure, and information on DIC parameters, as well as noise and uncertainty estimation related to the results presented in Chapter 3. Appendix B provides the MATLAB code used to consolidate the experimental data, match the data from the mechanical testing and DIC analysis, and calculate the parameters of interest such as stress, Poisson Function, and volume ratio.

1.4 Thesis Contributions

This thesis built upon prior research [7, 9, 14, 23, 24] to provide a quantitative method for evaluating the regional variation in brain tissue's anisotropy and compressibility. This method utilized two cameras to simultaneously analyze brain tissue samples from two perpendicular planes of view, allowing for the assessment of the PR and volume ratio changes in two different directions in response to uniaxial compressive strain at strains and magnitudes closer to TBI conditions. Given the ongoing debate concerning the presence of anisotropy in white matter [13], this research contributes valuable evidence regarding the variation in mechanical properties in the corpus callosum due to orientation of axon fibers. This knowledge ultimately increases confidence in the constitutive modeling of these tissues and their use in computational simulations.

Chapter 2

Background

This chapter provides an overview of relevant human brain anatomy and previous methods used for mechanical testing of both human and animal brain tissue. This chapter highlights the importance of understanding tissue compressibility and the role of uniaxial compression testing and Digital Image Correlation in advancing brain biomechanics research.

2.1 Neuroanatomy Overview

The brain is suspended in a protective cerebrospinal fluid (CSF) layer and fully enclosed by the skull [6]. This environment isolates it from the majority of the external loading experienced in daily life activities [6]. The complex and compliant cellular composition of brain tissue can be attributed to its unique function that prioritizes the processing and transmission of information over physical rigidity [30]. Thus, the brain's extracellular matrix (ECM) lacks load-bearing components like fibrillar collagen and elastin, containing instead non-fibrillar collagen types (e.g. IV and VI) that have limited contribution to structural support [31, 32].

The softness of brain tissue poses several challenges in its experimental investigation. These challenges include its sensitivity to handling and preparation before testing, the need for specialized equipment to assess its mechanical properties, and concerns about tissue dehydration during longer-term experiments [33]. This, com-

bined with the structural heterogeneity of brain tissue emphasizes the importance of understanding its composition to select relevant regions for testing to ensure reproducible results [14, 15, 34].

The brain can be broadly divided into three main components: the cerebrum, cerebellum, and brainstem. This brief overview will focus on the cerebrum, as it plays a critical role in higher cognitive functions and its prominence in brain biomechanics research [3]. The cerebrum is divided into two cerebral hemispheres, each of which is further segmented into four lobes: frontal, parietal, temporal, and occipital, as illustrated in Figure 2.1. These lobes are named after their nearest cranial bone and work together to perform the brain's higher functions [4].

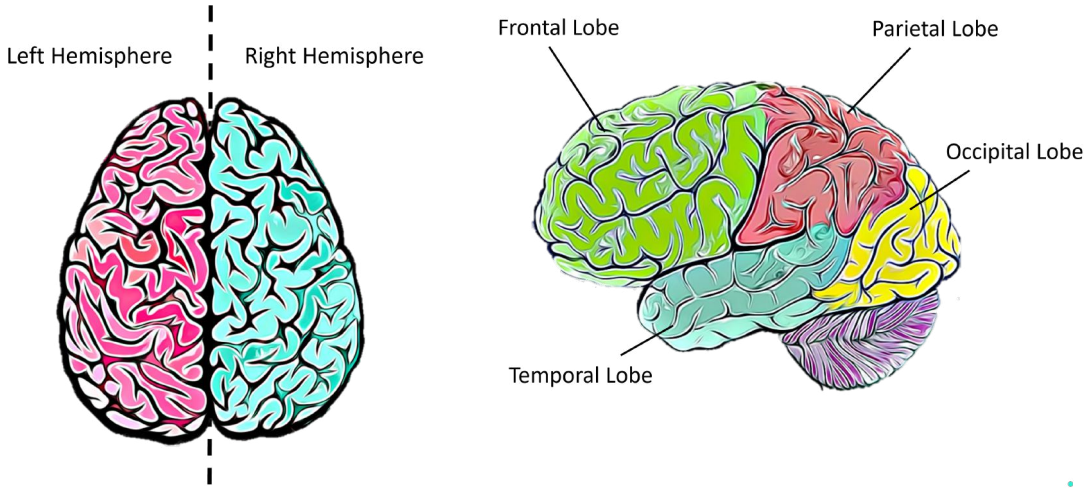

(a) Superior View (b) Lateral View

Figure 2.1: Anatomy of the human cerebrum.

At the macroscopic scale, brain tissue can be categorized as either gray or white matter [4]. The distinct locations of gray and white matter within the cerebrum are primarily due to the organization of neurons, the basic structural units of the brain [4]. Gray matter, responsible for processing and cognition, is situated in the brain cortex and is composed of neuron cell bodies [35]. In contrast, white matter, consisting of the axons that extend into the interior regions of the brain, enables communication between different brain regions [35].

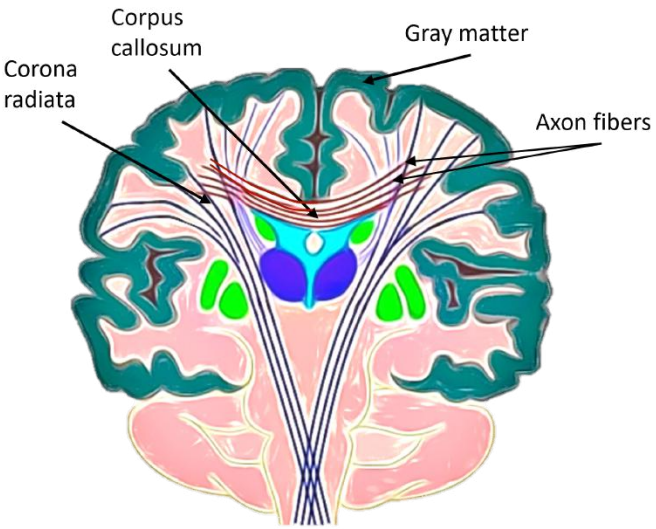

Figure 2.2: Coronal section of gray and white matter tissue depicting the axon direction in white matter. Corpus callosum has notably the most aligned fiber axon orientation.

The corpus callosum, a dense band of axon fibers predominantly made of white matter, serves as the physical link between the two cerebral hemispheres, facilitating essential signal transmission [4]. This region, densely packed with uniaxially oriented neuron axons, differs from the less organized white matter arrangement in other cerebral regions [4], as illustrated in Figure 2.2.

2.2 Clinical Significance of Brain Tissue Mechanics in Traumatic Injuries

Despite the protection provided by the skull and cerebrospinal fluid (CSF), the brain's soft composition allows for large deformations in response to external forces [8, 24]. Traumatic brain injuries (TBIs), for instance, result from rapid displacements in the tissue caused by external forces, leading to physiological disruptions in brain function [4, 36]. On the other hand, conditions such as hydrocephalus involve a slow dilation of brain ventricles, compressing surrounding tissue, and increasing intracranial pressure [3].

Traumatic brain injuries are a predominant cause of mortality and disability in

young adults and children [37]. Classified into primary and secondary lesions, these injuries have distinct characteristics [29, 38]. Primary lesions stem from rapid traumatic forces, such as contusions, while secondary lesions result from diffuse brain swelling, edema, displacement, or other subsequent effects following the initial impact [29]. This demonstrates the wide range of deformation rates experienced by the brain.

While both open-head and closed-head trauma scenarios exist, the majority of human TBIs result from impact to an intact skull, making investigations into closed-head injuries highly relevant [38]. Unlike open-head injuries where it is possible to observe and assess the extent of damage, closed-head injuries rely on observed symptoms, medical experience, and medical imaging such as CT and MRI [39, 40]. Unfortunately, the currently approved medical imaging protocols do not always provide a comprehensive view of the effects of an injury [40].

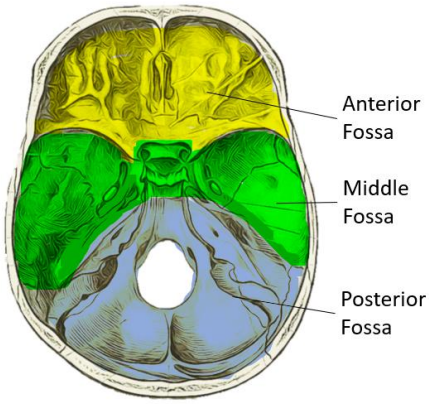

Figure 2.3: Cranial floor anatomy with distinct fossae highlighted for clarity. The anterior fossa is denoted in yellow, the middle fossa in green, and the posterior fossa in blue.

During closed-head trauma, primary lesions most commonly include Diffuse Axonal Injury (DAI) and cortical contusions [29]. DAI arises from shearing forces that tear nerve fibers in the brain's white matter tracts, frequently affecting the corpus callosum [29]. Contusions primarily affect the superficial cortex of the brain, leaving the

underlying white matter relatively unharmed. The cranial fossae, illustrated in Figure 2.3, closely envelop the brain within the skull. Even though the CSF acts as a shock absorber between the skull and brain, sudden changes in acceleration can cause the brain to impact the ridges between the fossae [41]. The cortical temporal lobe is commonly injured due to its proximity to the protruding sphenoid bone, located in between the middle and anterior cranial fossae [41]. Clinical studies on cerebral trauma have observed that the degree of post-traumatic atrophy appears to correlate with the severity of the trauma [41]. Therefore, gaining a deeper understanding of the mechanical properties of brain tissue can help improve the mathematical and computational models used in the development of diagnostic tools and injury thresholds [42], and reduce the short- and long-term complications associated with brain injuries [43].

2.3 Mechanical Testing of Brain Tissue

Previous studies have investigated the material properties of brain tissue, encompassing both in-vivo and ex-vivo research [44]. However, ethical considerations significantly constrain the feasibility of conducting in-vivo tests and the availability of fresh human brain tissue samples [3]. Consequently, the field heavily relies on ex-vivo and animal tissue experiments to advance the understanding of brain tissue mechanics [7].

Early work on brain mechanics was focused on understanding the mechanisms of injury during traumatic events [45]. However, with a growing emphasis on monitoring the progression of secondary traumatic brain injuries, and the advancements in robot-assisted and other surgical techniques, there is a broader interest in studying tissue behavior under slower-rate deformations to optimize treatment procedures [46].

Based on a continuum mechanics approach, studies often adopt a hyperelastic and incompressible constitutive formulation to describe the stress-strain behavior of brain tissue [47]. Hyperelastic modeling is particularly useful in analyzing short time scale events where materials undergo large, rapid deformations, borrowing from the time-

independent, non-linear constitutive formulation of rubber materials [21]. However, it has been shown that if the applied deformation rate is sufficiently slow, the tissue's local volume can change relative to its initial state due to fluid movement within or out of the tissue [13].

Brain tissue can experience complex loading conditions at a wide range of strain rates as a consequence of traumatic events or illness [33]. For that reason, various experimental methods have been used to investigate its mechanical behavior, including uniaxial compression and tension, shear, indentation, and Magnetic Resonance Elastography (MRE) [33]. Among these, uniaxial compression and tension tests are the most prevalent in the literature [3]. Animal tissues from sources such as bovine, porcine, and rodent brains are commonly used for these experiments [3].

The lack of consistency in experimental protocols, even within specific loading modes, makes it challenging to establish a consensus regarding the mechanical properties of brain tissue [48]. An important part of a protocol is the decision to include preconditioning prior to testing or not. Tissue preconditioning is typically employed for tissues that undergo cyclic loading in vivo, such as ligaments, tendons, myocardium, etc [49]. Its original purpose is to replicate the loading condition that simulates the in vivo environment during ex-vivo studies, and to achieve a stable and reproducible response, thereby minimizing the statistical variability of the measurements [49]. However, the brain tissue response of interest during TBI is after a single perturbation. Since the suggestion is to perform the preconditioning at the same strain magnitude as the maximum strain magnitude in the study [50], the risk of causing unintended tissue damage outweighs the benefits since the tissue in its original environment does not experience this type of large deformation cyclical loading.

In some studies, brain tissue is adhered to the test apparatus to prevent the sample from deforming under its own weight [7]. However, this approach requires more handling and tissue preparation, raising the risk of damaging the samples before testing [10]. Adhering the test specimens also restricts the lateral deformation at the

tissue boundaries, introducing stress concentrations, and causing a barreling effect that invalidates the uniaxial conditions of the test [14]. Furthermore, testing for regional variations in brain tissue requires small sample dimensions due to constraints such as the cortical layer's thickness of approximately 5 mm for gray matter, and the varying height of the corpus callosum, ranging from 3.65 mm to 10.92 mm [7, 51]. These dimensions limit the surface area available for strain measurement and increase the likelihood of capturing atypical deformations caused by stress concentrations at the adhered boundaries of the samples during DIC analysis [14].

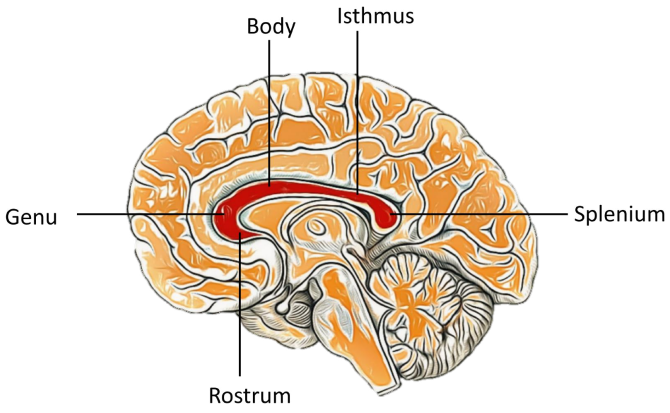

Figure 2.4: Diagram of a sagittal brain section highlighting the regions of the corpus callosum

While studies indicate variations in tissue properties across different brain regions, there is still a need for clarity as the reported trends are not always consistent [52], and the observed differences in properties in these studies are subtle and do not reach statistical significance [7, 9]. Nevertheless, there is a consensus among studies that brain tissue demonstrates a non-linear relationship between stress and strain, and this relationship is dependent on the loading rate [44].

2.3.1 Compressibility of Brain Tissue

Brain tissue, like many highly hydrated soft tissues, is often assumed as incompressible or nearly incompressible due to its high water content [20]. Few studies

have investigated the extent of the validity of this assumption. For example, Voyiadjis and Samadi-Dooki [13] fitted compressible and incompressible versions of the Ogden hyperelastic model to analyse the experimental results from Budday et al. [7] which tested human brain tissue at quasistatic strain rates in compression, tension and shear. They concluded that the tissue can be considered incompressible in compression since they found a volume change ratio of less than 1.2% at a compressive stretch ratio of 0.9. In tension, they found the tissue to be slightly compressible with a volume change of 5% for a 1.1 stretch ratio. Libertiaux et al. [23] measured the volume change of tissue experimentally by applying 3D DIC analysis to evaluate the evolution of the volume ratio of cylindrical brain samples of mixed white and gray matter under quasistatic uniaxial compression up to 0.12 strain. They conclude that under such conditions, the tissue can be considered incompressible as the volume ratio remains constant at approximately 1 throughout the tests. Their analysis provides valuable data, but their use of mixed gray and white porcine brain tissue cannot provide insight into regional variation in compressibility.

The vast majority of experimental studies have evaluated brain tissue compressibility by examining the Poisson's ratio (PR) [8, 14, 23, 24]. PR is defined as the negative ratio of the lateral strain to the axial strain during uniaxial tests [25]. The PR of soft solids is often characterized by compression tests due to experimental challenges encountered when fixing the sample surfaces to the test equipment to facilitate tension testing [53]. At infinitesimal strains, incompressible or nearly incompressible materials are found to have a PR of close to 0.5, but studies have shown that under finite strains, the PR becomes a nonlinear function of the axial strain [54].

At small strains, the PR values across various strain definitions are similar. However, at large strains, the PR given by the different strain definitions differ significantly. These differences become particularly pronounced and can critically impact the interpretation and application of the PR in scenarios involving large deformations. For example, Figure 2.5 shows the different PR values of a homogeneous isotropic and

incompressible material as a function of axial stretch, as defined by the Cauchy (Engineering), Green, and Hencky (True) strain definitions [54].

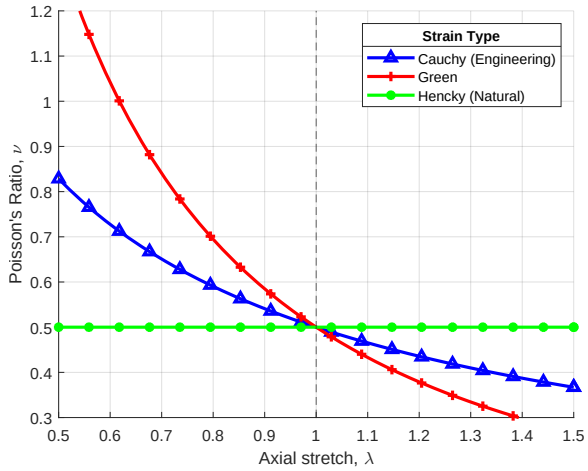

Figure 2.5: Poisson's ratio, ν, as a function of axial stretch, λ, for idealized incompressible materials according to Cauchy, Green and Hencky strain definitions

Examining Figure 2.5 reveals that the PR only remains constant at 0.5 for the Hencky or true strain scenario. Conversely, the PR is variable in the Cauchy or Green strain case. However, the true strain definition uses a spatial frame of reference, meaning that the reference changes with time, whereas the Green and Cauchy strain definitions use a material frame of reference that describes the deformation with respect to the original configuration [55]. Therefore, caution must be used when defining the PR in a study.

Eskandari et al. [24] optically measured the surface strains on cubical samples of bovine white matter brain tissue during uniaxial compression tests. They found that when compressing the tissue up to 30% strain, the average obtained PR value was 0.67 ± 0.05. The value exceeding $\nu = 0.5$ was attributed to a volume increase caused by damage or anisotropy in the tissue. However, even though unspecified in their study, they may have used the engineering (Cauchy) strain definition, which according to Figure 2.5, at a strain of 0.3 or compressive stretch of 0.7, the PR value is 0.65, closely matching their experimentally obtained value.

Felfelian et. al [14] investigated the anisotropic behavior of sheep brain stem and

corona radiata when compressed up to 15% strain at strain rates of 1/60 and 1/6 /s. They used Digital Image Correlation (DIC) to non-obstructively measure the transverse and axial strains during testing. They adhered the samples to the test setup due to the samples' pliable nature. Their results show average PR values of approximately 0.5 for both regions at both strain rates, thus concluding that the tissue could be considered incompressible. Additionally, they performed a Finite Element (FE) analysis using their fixed boundary conditions and compared their results to the obtained constants obtained by curve fitting their results to the Ogden hyperelastic model. The Ogden model assumes uniaxial compression and therefore unconstrained top and bottom faces [21]. Their comparison concluded that using the Ogden model in its standard form for the determination of material parameters is unsuitable for tests involving adhered surfaces.

These studies provide valuable data and demonstrate the potential of utilizing uniaxial compression in combination with optical techniques like DIC for assessing tissue compressibility. However, significant knowledge gaps persist in the literature. There is still an insufficient amount of data regarding the impact of factors such as the tested region, axon direction, and the effect of higher strain rates on tissue compressibility. Furthermore, these investigations have primarily employed animal tissues for PR and volume ratio studies, while providing only final or average values. Considering the non-linear nature of brain tissue, it would be particularly beneficial to explore the PR and compressibility evolution over the course of the deformation.

2.3.2 Relevance of Parameters Obtained from Uniaxial Compression Testing and DIC Analysis

Hyperelastic constitutive laws are commonly used to describe the macroscopic and time-independent deformation of brain tissue [7, 16, 47, 56]. Among the various hyperelastic energy functions, the Ogden model is often considered suitable for modeling brain tissue [7, 21, 47]. The following equation represents the strain energy density

function W for an Ogden model of hyperelastic material [2]:

$$\begin{aligned} W^{\mathrm{Ogd}} &= W_{\mathrm{iso}}^{\mathrm{Ogd}} + W_{\mathrm{vol}}^{\mathrm{Ogd}} \\ &= \frac{2\mu}{\alpha^2}\left[\tilde{\lambda}_1^{\alpha} + \tilde{\lambda}_2^{\alpha} + \tilde{\lambda}_3^{\alpha} - 3\right] + \frac{K}{4}\left[J^2 - 1 - 2\ln J\right], \end{aligned} \tag{2.1}$$

where W^{Ogd} is typically decomposed into an isochoric part $W_{\mathrm{iso}}^{\mathrm{Ogd}}$ and a volumetric part $W_{\mathrm{vol}}^{\mathrm{Ogd}}$. The terms $\tilde{\lambda}_1, \tilde{\lambda}_2, \tilde{\lambda}_3$ are the deviatoric stretches, which are modifications of the principal stretches that account for changes in shape without a change in volume. The parameter μ and α are material constants related to the deviatoric (or distortional) response of the material, indicating its resistance to shearing and its non-linear elastic behavior. The bulk modulus, K, is related to the volumetric response and represents the material's resistance to uniform compression. Lastly, J is the determinant of the deformation gradient tensor, which quantifies the change in volume of the material element; $J = 1$ indicates no volume change, $J > 1$ indicates a volume expansion, and $J < 1$ indicates a volume compression. In many brain modeling efforts, J is assumed to be equal to unity [13]. In other words, the tissue is considered incompressible, leading to the omission of the second term of Equation (2.1).

Given the difficulty of directly measuring the bulk modulus experimentally, the tissue compressibility is usually assessed by examining the Poisson's ratio (PR) [53]. However, in the case of anisotropic deformations, the theoretical limit of $PR \leq 0.5$ is not applicable [57]. Notably, no investigations have been conducted regarding the influence of region, strain rate, strain magnitude, and axon direction on the compressibility behaviour of brain tissue, nor the evolution of its Poisson's ratio as a function of strain to assess the limit of validity in the incompressibility approximation. Such research would help better determine whether anisotropic effects are present, which is essential when deciding whether to use isotropic or transverse isotropic models for these biological tissues [13].

Chapter 3

Optical Measurement of Human Brain Tissue Mechanical Properties Under Compression

3.1 Introduction

The brain is one of the softest tissues in the human body [34]. Due to its soft nature, it is capable of experiencing large deformations when exposed to mechanical loading, making it susceptible to injury from traumatic events or illness [58]. Traumatic brain injury (TBI) is a major concern as it is the leading cause of death in children and young adults [59, 60]. In the literature, finite element (FE) models have been utilized to study TBI and assess the extent of injury during a wide range of loading scenarios such as falls [61], sports injuries [62], or blast [63]. Such models are becoming more sophisticated as computational resources improve, but the identification of appropriate material properties and failure behaviors of biological materials is a primary focus in research efforts [3, 13, 64–66]. Comparing the output of models that use appropriate tissue properties to relevant trauma cases would provide insights into the load transfer and injury mechanisms within the tissue that can be used to improve existing injury diagnostic tools [67] and treatment strategies [43].

Studying the in-vivo deformation characteristics of brain tissue presents a range of ethical and logistical challenges [60]. Consequently, a variety of ex-vivo tests, such

as uniaxial compression [68, 69], tension [17, 46, 70], shear [71, 72], indentation [73, 74], and a combination of these [7, 9, 75] have been conducted using brain tissue samples sourced from bovine [73, 76], porcine [10, 37, 68, 69], rodent [37, 77], and, less commonly, human donors [7–9, 15, 52, 78]. Loading rates tested in such experiments range from quasi-static [7, 68] to dynamic [9, 69], and for strain magnitudes from 10% [7, 10] to 50% [9, 69]. Differences in sample preparation like the use of a variety of fluids for tissue hydration (e.g.phosphate buffered saline [7] or artificial cerebrospinal fluid [33]), different tissue geometries (cuboid [18] or cylindrical [68]), and differences in boundary conditions (adhered [52], or not adhered [18] sample surfaces to loading platen) complicate establishing a consensus on the mechanical properties of the tissue. However, a majority of studies agree that brain tissue exhibits non-linear and rate-dependent behavior [7, 9, 10, 68, 69].

One primary challenge in characterizing the mechanical behavior of the brain is attributed to the complex anatomical organization of the tissue. Macroscopically, brain tissue can be divided into gray and white matter [18]. Gray matter, predominantly found in the cerebral cortex, is composed of neuronal cell bodies, while white matter is located in the brain's interior where interconnected myelinated axon fibers allow for rapid cellular communication throughout the brain [3]. Recent literature highlights the importance of distinguishing between tissue types in the study of mechanical properties to enhance the understanding of brain tissue mechanics [7, 9, 14, 33]. Studies that distinguish between different brain tissue types predominantly characterize gray matter as both structurally and mechanically isotropic [7, 16, 18]. Conversely, it is hypothesized that the structural variability of the axon fibers in the white matter contributes to the variation in mechanical properties reported in the literature [3, 79]. For instance, some studies regard white matter as stiffer than gray matter [18, 73], others as softer [7], and others observe no difference [9, 15, 16].

Histology and diffusion tensor imaging (DTI) studies have established that the white matter region bridging the left and right hemispheres, called the corpus cal-

losum, consists of densely packed and uniaxially oriented axon fibers [7, 15, 16]. Therefore, this region presents a unique opportunity for investigating the role of axon direction on the tissue's mechanical behavior [14]. Studies using animal surrogate tissue have suggested the presence of mechanical anisotropy in porcine corpus callosum and brain stem when tested under shear [15, 16, 80], indentation [16], tension [17], and compression [18]. In human brain tissue studies, anisotropy in the corpus callosum was observed when tested in shear at a high deformation rate and magnitude [9], but a subsequent study did not find any directional dependencies when testing in compression, tension, and shear at low strain rate and comparatively small (10%) strain magnitude [7]. Even though both animal and human studies provide valuable contributions to the understanding of the material properties of brain tissue, the extent to which mechanical properties depend on the species is not well understood, complicating the application of animal results for the development of diagnostic and treatment tools for human brain lesions [37, 44].

Hydrated tissues, such as brain tissue, are often assumed incompressible or nearly incompressible due to their high water content [7, 8, 13, 20]. However, experimental data supporting the assumption of incompressibility for brain tissue are lacking. The elastic, time-independent response of brain tissue is commonly modeled as a hyperelastic material [81]. The measure for compressibility in brain constitutive modeling is given by the bulk modulus, but due to the challenges associated with the experimental measurement of volumetric deformation under hydrostatic stress, the Poisson's ratio (PR) has been investigated instead [53]. A PR of 0.5 is a common idealization in brain tissue modeling as an incompressible material [23, 33, 37, 52]. The PR is assumed to be a constant elastic property of a material, defined as the negative ratio of the strain in the transverse direction to the strain in the direction of loading. Recently, non-contact measurement techniques such as digital image correlation (DIC) have been used to investigate the PR in brain tissue during unconfined compression studies [14, 23, 24]. Optical techniques were used to compute the PR

of quasistatic compression tests up to 15% strain on bovine and sheep white matter brain tissue [14, 24]. Their results indicated an average final PR value of approximately 0.5, meaning that the material can be considered as nearly incompressible in these conditions. Conversely, a PR of 0.67 was obtained when testing in compression up to 30 % strain [24], potentially pointing to anisotropy effects or the formation of defects or voids leading to tissue damage as the strain is increased. The PR has largely been regarded as a fixed, constant value in the aforementioned investigations, so only final PR values at the maximum strain tested have been presented. Nevertheless, visualizing the PR evolution with strain would enable investigators to assess the extent of the validity of incompressibility assumptions more comprehensively. 3D DIC has been previously used to evaluate the evolution of the volume ratio of cylindrical brain samples of mixed white and gray matter under quasistatic uniaxial compression up to 0.12 strain [23]. Their findings indicate that under such conditions, the volume ratio remains constant at approximately 1 throughout the tests. However, their methods assumed isotropic deformations that inherently remove the ability to assess the presence of anisotropy in the tissue. Therefore, the knowledge gap that persists regarding the influence of factors such as region, strain rate, strain magnitude, and axon direction on the stress-stretch and compressibility behavior of brain tissue will be addressed here. Such factors are important for further consideration since the incompressibility assumption is used in FE models regardless of loading case [7, 69, 82], which can significantly influence the model predictions. To date, only animal tissues have been used in PR and volume ratio experimental investigations [14, 23, 24]. Furthermore, DIC studies that investigate the compressibility of the corpus callosum are missing from the literature. Such studies would be valuable for identifying the presence of anisotropy, while also providing a more comprehensive analysis of the applicability and limitations of the tissue incompressibility assumptions used in the literature. This study addresses these gaps and issues.

Building on previous studies [14, 23, 24], the objective of this work is to system-

atically investigate the stress-stretch behavior and compressibility of human brain tissue, with a focus on differences between gray and white matter, the influence of strain rate, and the effects of axon fiber direction up to strains of 30% (or a stretch ratio of 0.7). Uniaxial compression testing was carried out on cortical gray matter from the temporal lobe and white matter from the corpus callosum using a micromechanical testing apparatus at strain rates of 0.05 and 5 s^{-1}. To monitor the surface strains, two high-speed cameras were used in conjunction with DIC analysis to obtain surface strain information in perpendicular planes. The axial and transverse strains were used to compute and track the PR evolution in the two planes to assess the compressibility of all tissues and possible anisotropy of the white matter. The volume ratio was also calculated from these strains to assess the extent of the validity of compressibility assumptions. This study hypothesizes that the unidirectional axon fibers present in the corpus callosum contribute significantly to the anisotropic behavior of neural tissue, as suggested by previous studies [13]. Previous investigations on the tensile response of anisotropic tissues have established that the presence of anisotropy results in the PR depended on the loading direction [83]. Accordingly, this research proposes that examining the PR evolution of brain tissue at perpendicular planes could yield a more comprehensive understanding of the tissue mechanics, necessary for improving displacement predictions obtained from finite element simulations [2].

3.2 Materials and Methods

3.2.1 Specimen Extraction

Brain samples were extracted from 8 embalmed (formalin-fixed) cadavers from the University of Alberta Anatomical Gift Program. The methods and protocols described in this study were approved by the University of Alberta Research Ethics Board (ID: Pro00135530). The embalming process utilized a solution consisting of 4% phenol, 4% formalin (37% concentration), 8% glycol, 8% ethyl alcohol (95% concen-

tration), and 76% water. The brains were immersed in this solution for approximately 1 year. Cylindrical samples measuring 6 mm in diameter and 4 mm in height were excised using a biopsy punch (Electron Microscopy Sciences, Hatfield, PA). Tissue specimens coming from gray matter in the temporal lobe (TL) cortex and white matter samples in the corpus callosum (CC) were collected to determine regional variations in mechanical properties. Brains were cut in half along the sagittal plane, separating the two hemispheres. Samples from the CC to be tested along the fiber direction (CCwF) were extracted in the lateral-medial direction while samples to be tested perpendicular to the fiber direction (CCxF) were extracted in the superior-inferior direction. TL samples were extracted in a direction normal to the cortical surface. Figure 3.1 illustrates the sample configurations and fiber orientations during the compressive loading tests. Table 3.1 summarizes the number of samples tested from different brain regions at varying loading rates.

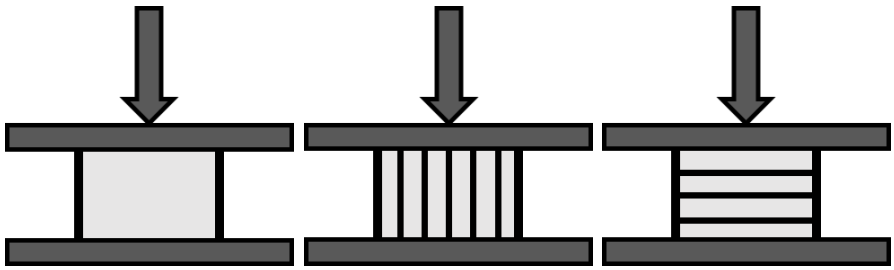

(a) TL (b) CCwF (c) CCxF

Figure 3.1: Schematic representation of tissue sample orientations for compression testing showing: a) temporal lobe (TL); b) corpus callosum with axons oriented parallel to the loading direction (CCwF); c) corpus callosum with axons oriented perpendicular to the loading direction (CCxF). Downward arrows indicate the direction of the applied compressive load.

3.2.2 Experimental Setup

Uniaxial compression tests were conducted using a Mach-1™ Micromechanical Testing System (BIOMOMENTUM, Quebec) equipped with a 17 N load cell which has a force resolution of 0.85 mN. Phosphate buffered saline (PBS) solution was applied between the specimen and loading platen surfaces to minimize frictional effects. Exper-

Table 3.1: Summary of samples per brain obtained for uniaxial compression experiments.

Brain nos.	Loading rate	Region tested		
		TL	**CCwF**	**CCxF**
I, II	0.05 s^{-1}	4	4	4
III, IV	5 s^{-1}	4	4	4
V, VI	0.05 s^{-1}	4	4	0
	5 s^{-1}	4	4	0
VII, VIII	0.05 s^{-1}	4	0	4
	5 s^{-1}	4	0	4

iments were performed at room temperature under displacement rates of 0.2 mm s^{-1} and 20 mm s^{-1}, corresponding to strain rates of 0.05 s^{-1} and 5 s^{-1}, respectively. The acquisition rate of the Mach-1 was set at 1 kHz.

Two high-speed AOS PROMON U750 cameras directed at the sample were placed at approximately 90° with respect to each other to observe the macroscopic deformation of the specimen at orthogonal planes as shown in Figure 3.2a. To optimize image quality and data storage efficiency, the cameras were set to acquire images with a resolution of 1280 x 660 pixels at varying frame rates corresponding to the test speeds. A frame rate of 309 frames per second was utilized for tests at the 5 s^{-1} loading rate to eliminate motion blur, while a reduced frame rate of 30 fps for tests at 0.05 s^{-1} helped in preventing memory overloads and recording failures. Specimens were positioned normal to the optical axis of the cameras to minimize out-of-plane displacement errors. To eliminate specular reflections and provide uniform lighting, cross-polarized high-intensity LED lights were used. The cross-polarization technique consists of placing a linear polarizer between the light source and the test specimen,

and a second polarizer of perpendicular polarity between the specimen and the camera [84]. This method selectively attenuates the glare caused by specular reflections on the hydrated sample surface. At the same time, it enhances image contrast and spatial precision in the collected images without requiring extensive specimen surface preparation.

Digital Image Correlation (DIC) was used to obtain the axial and transverse strain fields in the specimen surface during compression testing. In summary, DIC is a non-contact technique that divides a region of interest (ROI) into subsets that are tracked as the specimen undergo deformation. This tracking relies on an optimization algorithm that utilizes the gray levels at each image to match the corresponding subsets in the deformed state to the reference image, and thus the displacement or strain field can then be computed. During the analysis, the zero-normalized sum of squared differences (ZNSSD) correlation method with optimized 8-tap splines interpolation was utilized to provide accurate measures while minimizing errors caused by offsets or scaling in lighting [85]. Incremental correlation was used for a more stable prediction in the presence of large deformations [86]. Rigid body motion was removed during post-processing to further eliminate the effect of minimal camera vibration during the experiments.

The gray matter is mostly composed of neuronal cell bodies that lack a specific spatial distribution or orientation [87]. Therefore, no alignment was specified during the testing of TL samples. Given the uniform fiber direction in the CC [7], samples were placed such that the axon fiber direction was parallel to one camera view and perpendicular to the other when testing CCxF samples.

Since the tissues are hydrated, a water-insoluble ink was uniformly sprayed using a fine-point airbrush, creating a highly contrasted speckle pattern. Once the specimen preparation and lighting environment were ready, the PROMON U750 cameras were used to capture the deformation processes of the specimens at the two prescribed strain rates.

The starting point of the tests was determined optically when the superior loading platen made contact with the tissue. To maintain sample hydration, PBS solution was periodically applied using a dropper. With each test duration being no longer than 10 seconds, no application during testing was required to ensure consistent sample hydration. Before testing, excess PBS solution was removed from obstructing the camera views by using a delicate-task wipe to prevent decorrelation in the DIC algorithm due to image distortion.

No preconditioning cycles were applied in this study as it could lead to non-recoverable changes in the material properties at large deformations [1]. The Correlated Solutions VIC2D 6 software [88] was used to produce the strain measurements. The arrangement of cameras and polarizers is presented in Figure 3.2a.

The surface of each sample was aligned with the cameras' focal plane. The ROI, as shown in Figures 3.2b and 3.2c, was selected based on the area sharply in focus, as determined by the camera software's focus assist feature (AOS Technologies AG) to minimize the sample curvature impact on the measurements [89]. Additionally, the upper and lower boundaries of the samples, where fluid accumulation could cause decorrelation, were also excluded from the ROI. For consistency, when testing CCxF samples, the axon fiber direction is aligned with the front camera.

3.3 Data Processing

3.3.1 Stress-stretch

The Green strains were obtained through DIC analysis. Green strains were used due to their suitability when dealing with finite strains [55]. The strains, ε_i, are converted to stretches as

$$\lambda_i = \sqrt{2\varepsilon_i^G + 1} \tag{3.1}$$

where $i = 1, 2, 3$ denote the principal directions as shown in Figure 3.2.

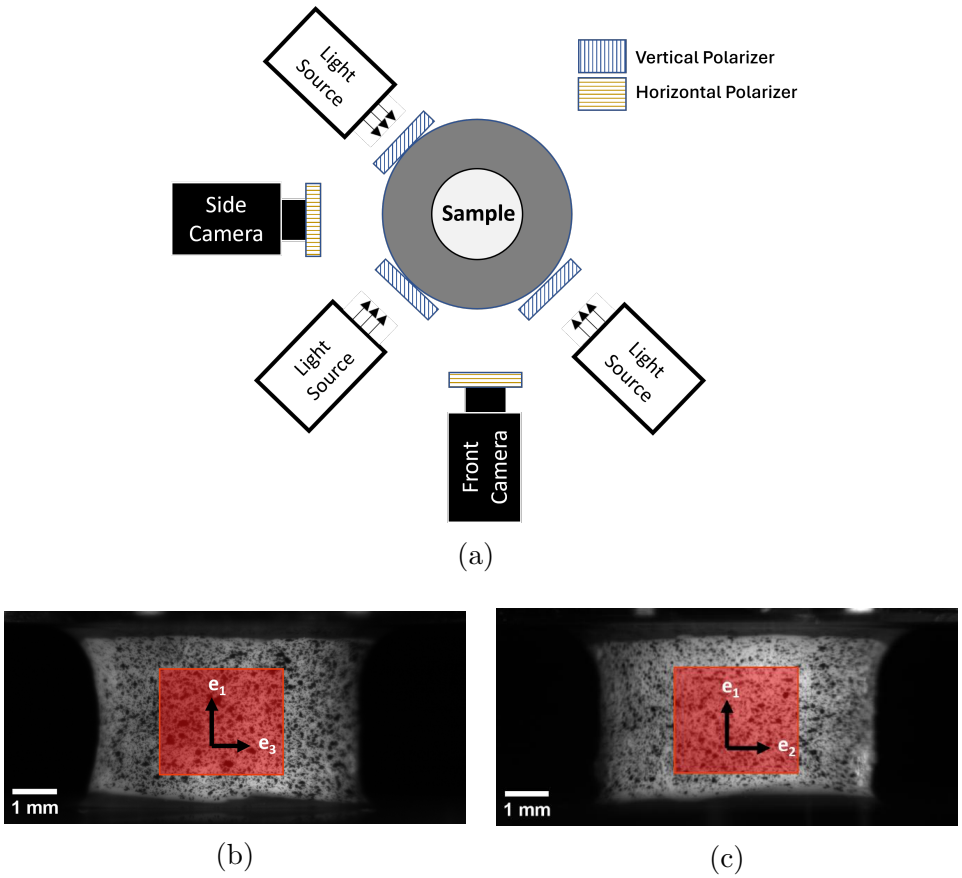

Figure 3.2: (a) Camera and polarizer arrangement for DIC implementation, (b) Compression of CCxF sample viewed along fibers (front camera), and (c) across fibers (side camera)

During the displacement-controlled experiments, the measured force, F, was converted to stress by $\sigma = F/A$, where A is the cross-sectional area of the specimen in the reference (unloaded) configuration. The stress-stretch response of the tissues is summarized for each region and loading rate.

3.3.2 Poisson Function

At finite deformations, the PR varies with axial strain or stretch, leading to the adoption of the term 'Poisson function' (PF) for a more appropriate description [13]. To investigate the anisotropy of brain tissue, values obtained in this study were compared to the ideal isotropic incompressible case. In the case of uniaxial compression of an isotropic incompressible material, for an arbitrary axial stretch ratio λ_1, it can be

assumed that $\lambda_2 = \lambda_3$. From the condition of incompressibility, $\lambda_1\lambda_2\lambda_3 = 1$, it follows that $\lambda_2 = \lambda_3 = \lambda_1^{-1/2}$. Therefore, for an incompressible homogeneous material, the PF is written as a function of the axial stretch [54] as

$$\nu(\lambda_1) = \frac{1}{\lambda_1^n + \lambda_1^{n/2}} \tag{3.2}$$

where $n = 1, 2$ gives the PF according to the Cauchy (or Engineering) and Green strain definitions, respectively.

3.3.3 Volume Ratio

In modeling hyper-elasticity, the elastic response of materials under large deformations is of particular interest. No material is perfectly incompressible, but this approximation has been widely used in the study of brain tissue [7, 69, 82]. The parameter for volume ratio, J, serves as an indicator of the compressibility of the material, where it is expected to remain close to 1 in incompressible cases. The volume ratio is calculated as

$$J = \lambda_1\lambda_2\lambda_3 \tag{3.3}$$

In such case, volume ratio vs axial stretch can be used to test the validity or the limits to the incompressible tissue assumption.

3.4 Experimental Results and Discussion

3.4.1 Uniaxial Compression

As shown in Figure 3.3, strain rate dependence is observed in all regions and loading cases, as demonstrated by the increased stress measured at increased strain rates and strain magnitudes. Regardless of the region and axon orientation, all curves exhibit a nonlinear stress-stretch response. From Figure 3.3, the stress-stretch curves for CCwF, CCxF, and TL samples fell within similar standard deviations, suggesting

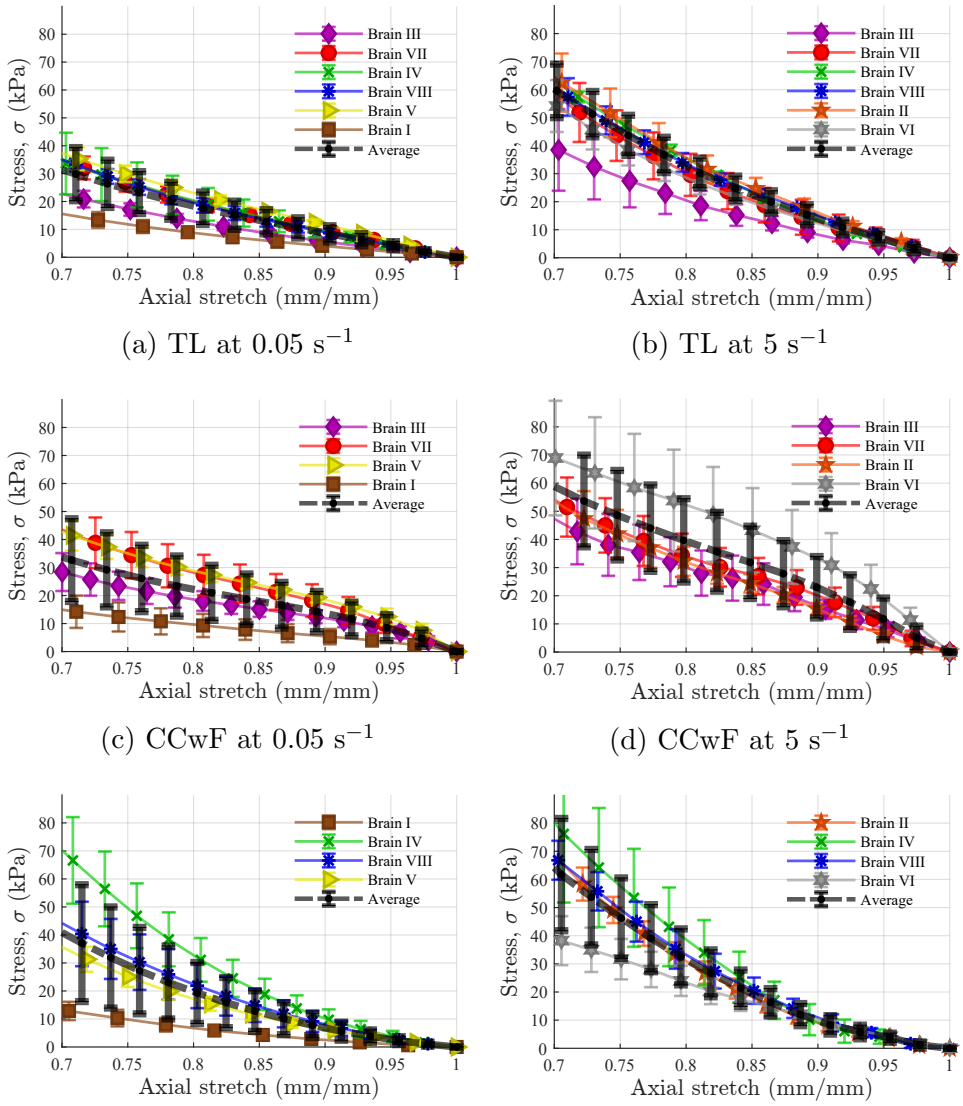

(a) TL at 0.05 s^{-1} (b) TL at 5 s^{-1}

(c) CCwF at 0.05 s^{-1} (d) CCwF at 5 s^{-1}

(e) CCxF at 0.05 s^{-1} (f) CCxF at 5 s^{-1}

Figure 3.3: Region-, orientation- and rate-dependent stress-stretch behavior for uniaxial compression experiments summarized in Table 3.1. The y-axis denotes the stress in kilopascals (kPa) and the x-axis represents the axial stretch. Different markers are used for different brain specimens. Each curve indicates the mean experimental values and associated standard deviations (error bars) obtained from four experiments.

a trend of consistent mechanical behavior across these tissues. In comparison with existing literature, the findings align with those reported by Jin et al. [9], who observed comparable mechanical properties in human white matter from the CC and corona radiata, and gray matter from the TL and basal ganglia. Their study highlighted that while white matter exhibited a slight increase in stiffness under compression, the

differences were not statistically significant. Similarly, Budday et al. [7] explored the mechanical properties of human brain tissue from the corpus callosum and corona radiata under various strain conditions. Their findings also showed no significant statistical difference in stiffness between gray and white matter. It is noted that the inclusion of preconditioning cycles in the latter study, as discussed by de Rooij and Kuhl [12], could potentially influence the initial fiber alignment in white matter samples, thereby affecting the comparability of results. The present study, while highlighting similar mechanical behavior trends across different tissue types, does not provide a statistical comparison of these differences, but rather contributes to the existing body of literature observing these trends.

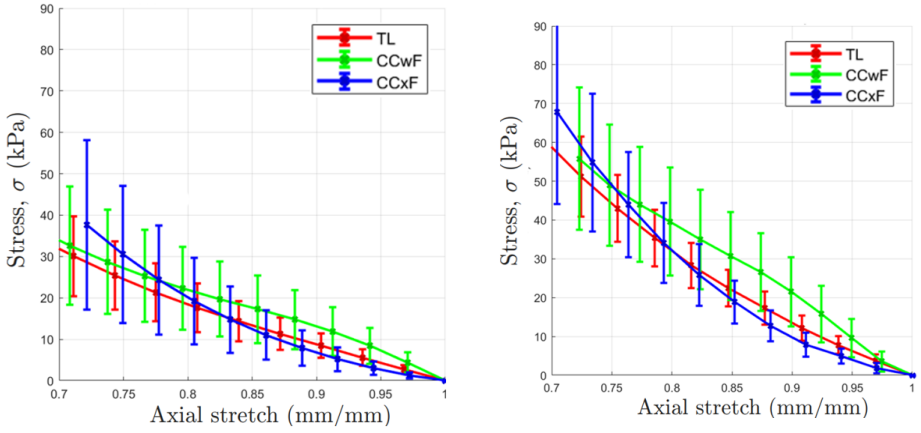

(a) TL, CCwF, CCxF at 0.05 s^{-1} (b) TL, CCwF, CCxF at 5 s^{-1}

Figure 3.4: Averaged stress-stretch results for uniaxial compression experiments. Each curve corresponds to the experimental values obtained by averaging all TL, CCwF, or CCxF experiments, respectively. Error bars represent the standard deviation.

The greater stiffness in white matter relative to gray is thought to result from the structural support provided by axon myelination [90]. Nevertheless, the primary role of myelin is associated with neural communication, and its impact on the mechanical properties of the brain remains under-investigated [90, 91]. Figures 3.3 and 3.4 do not show any clear differences among groups to establish whether axon fiber orientation influences mechanical behavior. To adequately assess the mechanical anisotropy of

the CC, the analysis should extend beyond stress-stretch relationships. Therefore, the next section presents the optical assessment of the evolution of the Poisson's Function (PF) to assess the trends in tissue isotropy and anisotropy.

3.4.2 Poisson Function (PF)

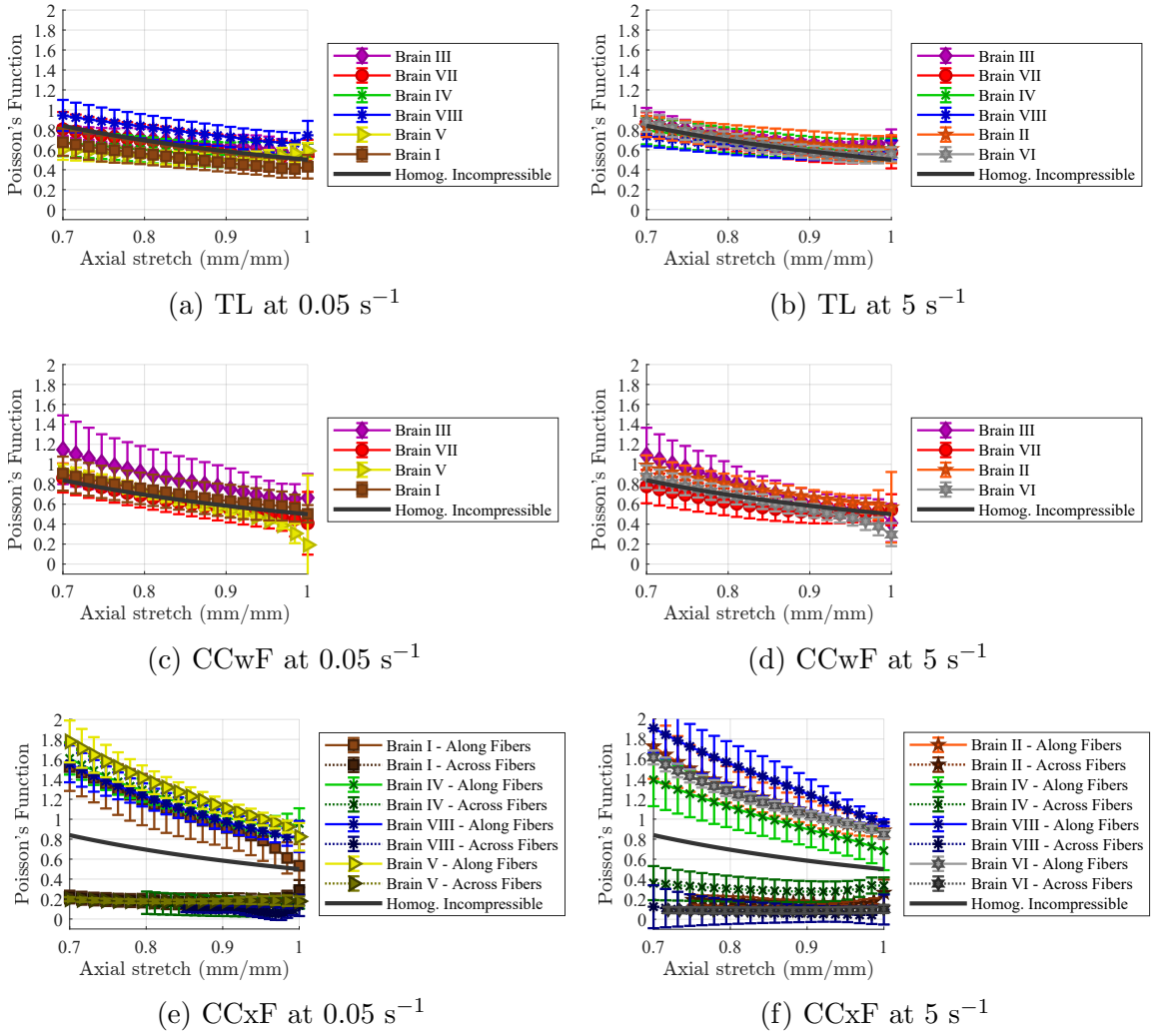

(a) TL at 0.05 s^{-1}

(b) TL at 5 s^{-1}

(c) CCwF at 0.05 s^{-1}

(d) CCwF at 5 s^{-1}

(e) CCxF at 0.05 s^{-1}

(f) CCxF at 5 s^{-1}

Figure 3.5: Region-, orientation- and rate-dependent PF results for uniaxial compression experiments at 0.05 and 5 s^{-1}. Different markers correspond to different brains tested. Curves indicate the mean experimental values and associated standard deviations (error bars) obtained from four experiments.

In Figure 3.5, the PF curve for an ideal homogeneous, isotropic, and incompressible material is presented alongside each plot for comparative purposes, as computed using Equation (3.2). The ideal curve illustrates that the PF, as defined by Green

strains, varies with axial stretch rather than remaining constant. This variation suggests that representing a non-linear material undergoing large deformations with a single Poisson's ratio value may not adequately capture its mechanical behavior.

The transverse stretches of the TL and CCwF samples in the two perpendicular planes of view (λ_2 and λ_3) showed similar responses. Thus, only the PF curves obtained from the transverse stretch (λ_2) and the axial stretch (λ_1) recorded by the front camera are displayed. As shown in Figures 3.5a to 3.5d, the PF curves for TL and CCwF at the two strain rates tested follow the general shape of the ideal curve. In Figure 3.5a, it can be observed that the curves for the TL samples tested at 0.05 s^{-1} exhibit a slight downward deviation from the ideal curve and this deviation becomes more apparent as the compression progresses. This trend is less apparent in the faster strain rate in Figure 3.5b, in which the average curve has a similar slope to the ideal curve. In the literature, slight compressibility of the tissue has been attributed to the displacement or reorganization of interstitial fluid within the hydrated tissue during slow or quasistatic displacement tests [8, 13]. Conversely, under faster rates, there is limited time for interstitial fluid reorganization. This results in minimal changes in tissue hydration during deformation, which in turn leads to less apparent compressibility.

Figures 3.5c and 3.5d show that the outcomes from both compression rates in the CCwF samples diverge slightly upward from the ideal curve. In the case of CCxF tissues in Figures 3.5e and 3.5f, the PF curves corresponding to the view aligned with the axon fiber direction were consistently higher than the ideal curve, while the opposite is true for the view perpendicular to the fiber direction. This consistent deviation from the idealized case depending on the plane analysed points to the presence of anisotropy in the corpus callosum.

Eskandari et al. [24] conducted quasistatic compression tests on bovine white matter tissue at strains of 5, 10, and 30%, obtaining PR estimates of 0.45, 0.47, and 0.67, respectively. The PR of 0.67 at 30% strain, was suggested to indicate potential tissue

damage or anisotropy. However, by computing the PR at 30% with Equation (3.2) using the engineering strain definition (setting $n = 1$) results in a PF of 0.65, closely aligning with their experimental 0.67, suggesting possible isotropic elastic behavior. While the findings from Eskandari et al. [24] offer valuable data on the PR of bovine white matter, it is important to note the limitation in focusing primarily on final PR values at specific strain magnitudes. A more comprehensive understanding of brain tissue mechanical behavior can be gained by investigating the evolution of PR across a range of strains, potentially providing deeper insights into tissue anisotropy or structural changes.

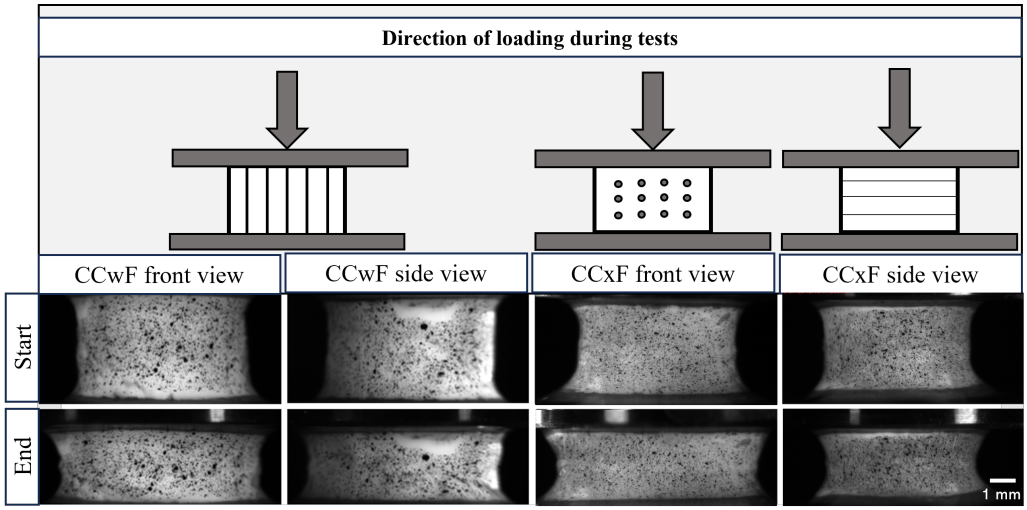

Figure 3.6: Speckled corpus callosum samples before (top row) and after (bottom row) compression. The front and side view correspond to different views of the same sample tested. Diagrams at the top depict the sample axon orientations during testing. In CCwF samples, the axons are mostly aligned superior-inferiorly. For CCxF samples, the front camera is aligned with the fiber direction of the sample, and the side camera is perpendicular to the axon direction.

As depicted in the two left columns of Figure 3.6, the CCwF samples exhibit uniform deformation in both observed planes. In contrast, the deformation of the CCxF samples differed depending on the observed plane of view, as presented in the two right columns of Figure 3.6. The CCxF samples deform preferentially in the direction perpendicular to the axon direction, and very little along the axon direction. The large discrepancy in transverse deformation explains the consistently wide discrep-

ancy in the PF curves for the CCxF tests, as observed in Figures 3.5e and 3.5f. This suggests that the tissue structure of the CC does influence its mechanical behavior by limiting deformation along the axon direction. The findings from the CCwF and CCxF tests suggest the CC exhibits transverse isotropy, characterized by an axis of symmetry that coincides with the axon fiber orientation [16]. The existence of this anisotropy also implies that the compressibility of the corpus callosum cannot be solely verified by examining the PF-stretch plots.

3.4.3 Volume Ratio

Despite the lack of conclusive evidence supporting the incompressibility of brain tissue, this simplifying assumption is commonly adopted in both analytical and numerical models [8, 82]. The compressibility of the CC could not be fully assessed using the PF curve due to the presence of non-homogeneous deformations. The volume ratio, J, is used to explore the elastic deformation and the potential limits of brain tissue's incompressibility assumption. Therefore, to fully characterize the anisotropic compressibility of a material, it is necessary to track how J changes in the different loading directions. The relationship between J and stretch for all tested regions and orientations is presented in Figure 3.7, where the mean results across all brain specimens for each loading condition are highlighted in black.

Similar trends can be observed for the TL when comparing the volume ratio in Figures 3.7a and 3.7b to the PF curves in Figures 3.5a and 3.5b. The TL tested at 0.05 s^{-1} shows a slight downward deviation from $J = 1$ as the compression proceeds. This downtrend is less apparent in the tests conducted at 5 s^{-1}. For the CCwF samples, the plotted J values deviate upward from the incompressibility limit of $J = 1$. The perceived increase in volume in the CC compressed along the axon fiber direction may suggest the potential generation of voids or other microstructural defects within the tissue as the tests proceed [68]. It is also apparent that this point of departure from $J = 1$ starts earlier as the strain rate is increased. Therefore, in this case, the limit at

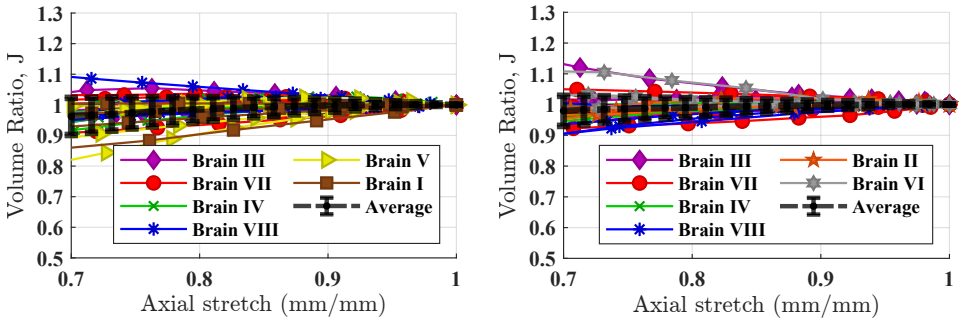

(a) TL at 0.05 s^{-1}

(b) TL at 5 s^{-1}

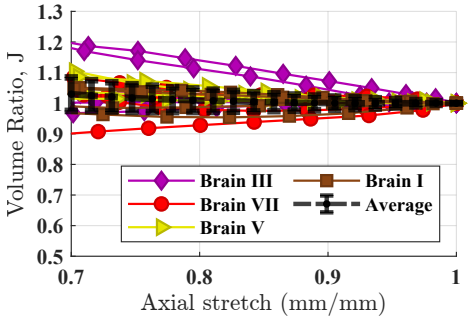

(c) CCwF at 0.05 s^{-1}

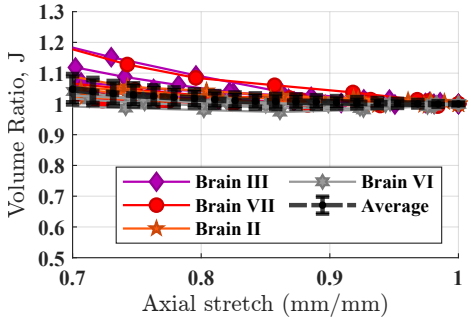

(d) CCwF at 5 s^{-1}

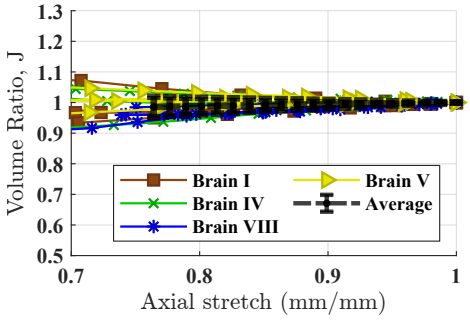

(e) CCxF at 0.05 s^{-1}

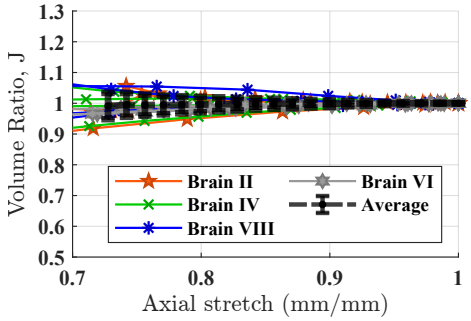

(f) CCxF at 5 s^{-1}

Figure 3.7: Region-, orientation- and rate-dependent J vs stretch results for uniaxial compression experiments. Different markers are used for different brain specimens. Each curve indicates the mean experimental values obtained from 4 experiments, and error bars represent the standard deviation.

which the incompressibility assumption would be valid is also strain rate dependent. Looking at the CCxF results presented in Figures 3.7e and 3.7f, the volume ratio curves are evenly distributed about $J = 1$, even though the corresponding PF curves presented in Figures 3.5e and 3.5f differed from the ideal curve. This demonstrates that the volume ratio parameter can be used to assess the compressibility of the tissue

even for anisotropic materials. However, it is important to note that even though the values scatter around $J = 1$, as shown by the average curve, there is non-negligible variability in the data.

Table 3.2: Comparison of J values at different strain rates for temporal lobe and corpus callosum regions

Region/Direction	**Rate**	$\mathbf{J}_{\lambda_{0.77}}$	$\mathbf{J}_{\lambda_{0.70}}$
TL	$0.05\ s^{-1}$	0.978 ± 0.046	0.962 ± 0.060
	$5\ s^{-1}$	0.988 ± 0.035	0.980 ± 0.049
CCwF	$0.05\ s^{-1}$	1.013 ± 0.042	1.029 ± 0.055
	$5\ s^{-1}$	1.024 ± 0.030	1.048 ± 0.046
CCxF	$0.05\ s^{-1}$	0.986 ± 0.032	-
	$5\ s^{-1}$	0.994 ± 0.031	-

From Table 3.2, several trends previously mentioned can be more objectively observed. The J values at a stretch of 0.77 are listed as this is the highest magnitude at which all tests were captured. Looking at this table it is easy to see that the J values increase with compression rate. The CCxF samples demonstrate a smaller increase in the mean J values with increased strain rate as compared to the TL and CCwF samples. Nevertheless, the difference between the TL and the CCxF are within one standard deviation from each other, implying their similarity within the measured strain rates. It is also evident that the J values at $\lambda_{0.70}$ are still within one standard deviation from $J = 1$, providing even more evidence that the significant deviation from $\nu = 0.5$ at an applied strain of 30% was most likely due to the inherent behaviour of the PR when using the engineering strain definition, rather than an increase in volume or damage in the tissue.

From this investigation, it is evident that the values of J do show variability from a value of 1. For the TL tests, for example, a conservative measure for the variability in the data can be the standard deviation which is ± 0.06 for the tests conducted at

0.05 s^{-1}. The effect of a change from $J = 1$ to $J = 1.06$ can be observed by referring to the strain energy density function, W. For nearly incompressible materials, the commonly used one-term Ogden strain energy density function, W^{Ogd} , can be decoupled into its isochoric and volumetric parts [2] as

$$W^{\text{Ogd}} = W^{\text{Ogd}}_{\text{iso}}(\bar{\lambda}) + W^{\text{Ogd}}_{\text{vol}}(J) \tag{3.4}$$

where the $W^{\text{Ogd}}_{\text{iso}}(\bar{\lambda})$, $W^{\text{Ogd}}_{\text{vol}}(J)$ are the isochoric and volumetric parts of the function. The isochoric part of the function is generally written as:

$$W^{\text{Ogd}}_{\text{iso}}(\bar{\lambda}) = \frac{2\mu}{\alpha^2}\left[\tilde{\lambda}_1^{\alpha} + \tilde{\lambda}_2^{\alpha} + \tilde{\lambda}_3^{\alpha} - 3\right] \tag{3.5}$$

where $\bar{\lambda}_i$ are the isochoric principal stretches, and μ and α are material parameters [92]. The volumetric part of W^{Ogd} would be affected by the volume change and is often modeled as

$$W^{\text{Ogd}}_{\text{vol}}(J) = \frac{K}{4}\left[J^2 - 1 - 2\ln J\right] \tag{3.6}$$

where J is the volume ratio and K is the bulk modulus. From Equation (3.6), when $J = 1$, $W^{\text{Ogd}}_{\text{vol}}(J = 1) = 0$, leaving only the isochoric strain energy term, $W^{\text{Ogd}}_{\text{iso}}(\bar{\lambda})$ shown in Equation (3.5). However, a change of ± 0.06 in J results in $W^{\text{Ogd}}_{\text{vol}}(J = 1 \pm 0.06) = 0.0018K$. In other words, $W^{\text{Ogd}}_{\text{vol}}$ represents the additional energy stored in the material due to its slight compressibility [93]. This can be significant in materials that are assumed to be perfectly incompressible, like many biological tissues including brain tissue, due to their characteristically high bulk modulus, K [66]. In the literature, bulk moduli of brain tissue range from 5.5 MPa to 5.5 GPa [66]. Using the conservative value of $K = 5.5MPa$, a deviation of $J = 1 \pm 0.060$ could lead to a change of $W^{\text{Ogd}}_{\text{vol}} = 9.7kPa$, resulting in a significant energy penalty, even for small volume changes. Therefore, when estimating the error tolerance asso-

ciated with the assumption of incompressibility in brain tissue models, it is important to consider the strain magnitude, loading rate, and tissue type.

3.5 Limitations

This investigation of the mechanical properties of brain tissue focused on the gray cortical matter of the temporal lobe. The temporal lobe region was chosen due to its frequent involvement in TBI events [41], while other cortical regions were excluded to minimize variations between samples. Examining and comparing multiple regions within a tissue type could reveal valuable property trends, such as stiffness variations in cortical gray matter from different regions that could show different properties due to non-uniform capillary density [7]. This study also used embalmed human brain tissue, affecting its mechanical response due to possible protein cross-linking, shrinkage, and dehydration [94]. However, the tissue retained its characteristic non-linearity and viscoelasticity, while stress values were approximately an order of magnitude higher than in comparable studies [9]. Limited by a maximum strain rate of $5s^{-1}$ due to equipment constraints, and the small size of the corpus callosum, future work could explore higher strain rates relevant to ballistic or blast conditions that are found to exceed $100s^{-1}$ [95]. Such studies are crucial for understanding TBI mechanisms and improving protective measures.

3.6 Conclusion

This study aimed to uncover mechanical behavior trends in human brain tissue under uniaxial compression and demonstrated a method to assess tissue compressibility in the case of anisotropic and large deformations. This study investigated the stress-stetch behavior, and evolution of the PR and volume ratio, J, in human brain tissue under uniaxial compression. Comparisons between gray cortical matter and white callosal matter were focused on the differences due to tissue type, strain

rates, and axon fiber orientations. Stress-stretch plots revealed an increase in the measured stress response with strain rate and magnitude, while similar results were observed when comparing tissue types and loading directions. Deviations from the ideal PF-stretch curves captured the anisotropic response in the corpus callosum, more specifically transverse isotropy, whereas the temporal lobe exhibited homogeneous deformations and only deviated slightly from the ideal incompressible model, showing that it can be considered a slightly compressible tissue.

Generally, J values indicated minimal compressibility, except in the CCwF samples where values higher than $J = 1$ suggest a volume increase, possibly caused by void formation within the tissue. These insights highlight the need for tailored models to accurately represent brain tissue behavior, especially considering no material is perfectly incompressible. This study contributes to a more accurate understanding of brain tissue mechanics, showing the need for transversely isotropic models of the corpus callosum to improve existing computational models dealing with large deformations as is the case for brain injury simulation for treatment and prevention [1, 12].

Chapter 4

Conclusions, Limitations, and Future Work

4.1 Conclusions

The objective of this thesis was to advance the understanding of the stress-stretch and compressibility behavior of brain tissue across different tissue types, strain rates, magnitudes, and loading directions using an experimental mechanics approach. The work in this thesis also focused on assessing the validity and the effect of assuming incompressibility in human brain tissue. Building on previous works [14, 23, 24], an experimental protocol that utilized Digital Image Correlation (DIC) was developed to investigate the mechanical properties of brain tissue during displacement-controlled uniaxial compression experiments.

This work systematically investigated the stress-stretch behavior and compressibility of human brain tissue by testing samples of gray matter from the temporal lobe and white matter from the corpus callosum, emphasizing the effects of strain rate and axon fiber direction on the uniaxial compression response at a stretch magnitude of approximately 0.7. Due to the small dimension required to obtain samples containing a single tissue type and the hydrated nature of the samples, a technique called cross-polarization was implemented for the first time in brain tissue DIC studies to minimize the time required to prepare sample surfaces for testing and analysis while also increasing image contrast and allowing for better adherence of the speckles

during testing. Surface deformations during testing were simultaneously measured in two perpendicular planes to examine the possible anisotropic behavior of the tissues.

The results showed that the measured stress response in brain tissue increased with strain rate and magnitude in all tested regions and directions. In the corpus callosum, variations in the loading direction relative to the fiber orientation had minimal impact on stress measurements, but PF curve analysis in two perpendicular planes revealed trends pointing to transversely isotropic behavior. The temporal lobe exhibited homogeneous deformation as demonstrated by the resulting PF curves that closely aligned with the ideal incompressible case.

The J-stretch plots showed that the compressibility of brain tissue depends on strain rate and magnitude. The temporal lobe and corpus callosum compressed along the fiber direction showed consistent trends in both PF-stretch and J-stretch plots. Conversely, the PF-stretch plots for the corpus callosum compressed across its fiber direction exhibited clear anisotropic behavior as demonstrated by the markedly distinct PF behavior when comparing both views. This showed that the PF-stretch plots alone are inadequate for assessing tissue compressibility. The variation in tissue behavior across different planes of view in the corpus callosum suggests that the diverse results regarding white matter behavior found in the literature could be due to the difficulty in obtaining similarly structured samples from other white matter cerebral regions with less organized axon fiber structures [14]. On average, the J values for TL and CCwF samples generally remained at or below $J = 1$, indicating minimal compressibility. In contrast, CCwF samples deviated consistently above $J = 1$ demonstrating a trend that suggested the formation of voids within the tissue. Using an Ogden model with the incorporation of slight compressibility, it was shown that the appropriateness of the ideal incompressibility assumption depends on the tissue region, the direction of loading, and the expected maximum strain rates and magnitudes.

These results highlight the importance of investigating variations in stiffness and

compressibility in different regions and directions of loading. As no material is perfectly incompressible, they should only be approximated as incompressible only once taken into account the errors that would result from said approximations. This study demonstrates that assumptions of perfect incompressibility could yield results within an acceptable error margin, depending on the specific tolerance levels. The methods presented enhance understanding of brain tissue compression and highlight the necessity for transversely isotropic models for CC samples, which is crucial for advancing computational models that aid in the treatment and prevention of brain injuries and disorders [1, 12, 72].

4.2 Limitations and Future Work

In this study, samples from the temporal lobe were utilized to assess the gray cortical matter behavior. This was based on the common involvement of the temporal lobe in TBI events [41], as well as the aim to minimize potential variations in properties that could arise from including other brain regions in the comparisons. Nevertheless, comparing the property variation among multiple regions from the cortical gray matter would provide valuable trends in mechanical properties. It has been hypothesized that non-uniform capillary density due to regional metabolic demands in the different cortical lobes could contribute to differences in the stress response when comparing cortical gray matter regions [7]. Another important limitation is the utilization of embalmed (or fixed) human brain tissue which inevitably influences its mechanical response and limits the information obtainable from these experiments to qualitative measurements. A previous study that measured the tissue stiffness changes during intracranial expansion tests on live, dead, and formalin-embalmed animal brain tissue found that, compared to in-vivo measurements, stiffness increases after fixation but the shape of the force-displacement curves remained unaffected [96]. This study showed embalming stiffens brain tissue, with stress responses one order of magnitude higher than literature values under similar conditions [9, 69]. However, this study

has shown that after fixation, brain tissue maintained a non-linear and viscoelastic behavior as exhibited by the noticeable strain rate dependence in all regions tested in this thesis work. Formaldehyde fixation causes cross-linking of proteins in the tissue, which changes its microstructure [94]. Even though brain tissue has a much lower collagen content relative to other tissues such as muscle and ligaments [47], the fixation process potentially impacts the degree of mechanical anisotropy as compared to fresh brain tissue [94]. These structural alterations must be carefully considered when extrapolating present findings to live or fresh tissue. Nevertheless, this thesis work aimed to identify qualitative trends regarding brain tissue behavior under uniaxial compression while showing a method to assess the validity of the incompressibility assumption, especially in the case of anisotropic deformations.

The thesis study was also constrained by a maximum strain rate of 5 s^{-1}, or displacement rate of 20 $mm\,s^{-1}$, due to the limitations of the available testing equipment and the small sample dimensions. Extending this methodology to testing at higher strain rates might uncover further trends than those presented in this thesis. A recommended direction for future research is the assessment of brain tissue behavior under ballistic or blast conditions, which correspond to strain rates exceeding 100 s^{-1}. The study of such high-rate scenarios is critical for the development of appropriate protective equipment and measures [95].

The knowledge obtained through this work could also be expanded by including tension and shear experiments to better characterize the tissue behavior in multiple loading modes, and better encapsulate the continuum mechanics approach with which the mathematical models are formulated. As hypothesized by Voyiadjis et al. [13], including the compressibility behavior to the constitutive formulation of these tissues could help capture the tension-compression asymmetry observed in experimental stress-stretch results [7].

Bibliography

[1] F. Eskandari, M. Shafieian, M. M. Aghdam, and K. Laksari, "A knowledge map analysis of brain biomechanics: Current evidence and future directions," *Clinical Biomechanics*, vol. 75, p. 105 000, 2020.

[2] E. Griffiths, J. Hinrichsen, N. Reiter, and S. Budday, "On the importance of using region-dependent material parameters for full-scale human brain simulations," *European Journal of Mechanics-A/Solids*, vol. 99, p. 104 910, 2023.

[3] S. Budday, T. C. Ovaert, G. A. Holzapfel, P. Steinmann, and E. Kuhl, "Fifty shades of brain: A review on the mechanical testing and modeling of brain tissue," *Archives of Computational Methods in Engineering*, vol. 27, pp. 1187–1230, 2020.

[4] J. W. Melvin and N. Yoganandan, "Biomechanics of brain injury: A historical perspective," in *Accidental Injury: Biomechanics and Prevention*, Springer, 2014, pp. 221–245.

[5] A. Greiner, N. Reiter, F. Paulsen, G. A. Holzapfel, P. Steinmann, E. Comellas, and S. Budday, "Poro-viscoelastic effects during biomechanical testing of human brain tissue," *Frontiers in Mechanical Engineering*, vol. 7, p. 708 350, 2021.

[6] L. Telano and S Baker, "Physiology, cerebral spinal fluid," *StatPearls*, 2023. [Online]. Available: https://www.ncbi.nlm.nih.gov/books/NBK519007/.

[7] S. Budday, G. Sommer, C. Birkl, C. Langkammer, J. Haybaeck, J. Kohnert, M. Bauer, F. Paulsen, P. Steinmann, E. Kuhl, *et al.*, "Mechanical characterization of human brain tissue," *Acta biomaterialia*, vol. 48, pp. 319–340, 2017.

[8] G. Franceschini, D. Bigoni, P. Regitnig, and G. A. Holzapfel, "Brain tissue deforms similarly to filled elastomers and follows consolidation theory," *Journal of the Mechanics and Physics of Solids*, vol. 54, no. 12, pp. 2592–2620, 2006.

[9] X. Jin, F. Zhu, H. Mao, M. Shen, and K. H. Yang, "A comprehensive experimental study on material properties of human brain tissue," *Journal of biomechanics*, vol. 46, no. 16, pp. 2795–2801, 2013.

[10] M Hrapko, J. Van Dommelen, G. Peters, and J. Wismans, "Characterisation of the mechanical behaviour of brain tissue in compression and shear," *Biorheology*, vol. 45, no. 6, pp. 663–676, 2008.

[11] M. Begonia, R Prabhu, J Liao, W. Whittington, A Claude, B Willeford, J Wardlaw, R Wu, S. Zhang, and L. Williams, "Quantitative analysis of brain microstructure following mild blunt and blast trauma," *Journal of Biomechanics*, vol. 47, no. 15, pp. 3704–3711, 2014.

[12] R. de Rooij and E. Kuhl, "Constitutive modeling of brain tissue: Current perspectives," *Applied Mechanics Reviews*, vol. 68, no. 1, p. 010 801, 2016.

[13] G. Z. Voyiadjis and A. Samadi-Dooki, "Hyperelastic modeling of the human brain tissue: Effects of no-slip boundary condition and compressibility on the uniaxial deformation," *Journal of the mechanical behavior of biomedical materials*, vol. 83, pp. 63–78, 2018.

[14] A. M. Felfelian, A. Baradaran Najar, R. Jafari Nedoushan, and H. Salehi, "Determining constitutive behavior of the brain tissue using digital image correlation and finite element modeling," *Biomechanics and Modeling in Mechanobiology*, vol. 18, pp. 1927–1945, 2019.

[15] M. T. Prange and S. S. Margulies, "Regional, directional, and age-dependent properties of the brain undergoing large deformation," *J. Biomech. Eng.*, vol. 124, no. 2, pp. 244–252, 2002.

[16] Y. Feng, R. J. Okamoto, R. Namani, G. M. Genin, and P. V. Bayly, "Measurements of mechanical anisotropy in brain tissue and implications for transversely isotropic material models of white matter," *Journal of the mechanical behavior of biomedical materials*, vol. 23, pp. 117–132, 2013.

[17] F Velardi, F Fraternali, and M Angelillo, "Anisotropic constitutive equations and experimental tensile behavior of brain tissue," *Biomechanics and modeling in mechanobiology*, vol. 5, no. 1, pp. 53–61, 2006.

[18] M. Hoppstädter, D. Püllmann, R. Seydewitz, E. Kuhl, and M. Böl, "Correlating the microstructural architecture and macrostructural behaviour of the brain," *Acta Biomaterialia*, vol. 151, pp. 379–395, 2022.

[19] M. Hosseini-Farid, M. Ramzanpour, J. McLean, M. Ziejewski, and G. Karami, "Rate-dependent constitutive modeling of brain tissue," *Biomechanics and modeling in mechanobiology*, vol. 19, pp. 621–632, 2020.

[20] K. Miller and K. Chinzei, "Constitutive modelling of brain tissue: Experiment and theory," *Journal of biomechanics*, vol. 30, no. 11-12, pp. 1115–1121, 1997.

[21] R. Ogden, *Non-linear elastic deformations*. Courier Corporation, 1997.

[22] M. Palanca, G. Tozzi, and L. Cristofolini, "The use of digital image correlation in the biomechanical area: A review," *International biomechanics*, vol. 3, no. 1, pp. 1–21, 2016.

[23] V Libertiaux, F Pascon, and S Cescotto, "Experimental verification of brain tissue incompressibility using digital image correlation," *Journal of the mechanical behavior of biomedical materials*, vol. 4, no. 7, pp. 1177–1185, 2011.

[24] F. Eskandari, Z. Rahmani, and M. Shafieian, "The effect of large deformation on poisson's ratio of brain white matter: An experimental study," *Proceedings of the Institution of Mechanical Engineers, Part H: Journal of engineering in medicine*, vol. 235, no. 4, pp. 401–407, 2021.

[25] B. J. Goodno and J. M. Gere, *Mechanics of Materials, SI Edition*. Cengage Learning, 2017, ISBN: 9781337093354.

[26] G. N. Greaves, A. L. Greer, R. S. Lakes, and T. Rouxel, "Poisson's ratio and modern materials," *Nature materials*, vol. 10, no. 11, pp. 823–837, 2011.

[27] S. K. Kyriacou, A. Mohamed, K. Miller, and S. Neff, "Brain mechanics for neurosurgery: Modeling issues," *Biomechanics and modeling in mechanobiology*, vol. 1, no. 2, pp. 151–164, 2002.

[28] E. G. Takhounts, R. H. Eppinger, J. Q. Campbell, R. E. Tannous, E. D. Power, and L. S. Shook, "On the development of the simon finite element head model," SAE Technical Paper, Tech. Rep., 2003.

[29] L. R. Gentry, J. C. Godersky, and B. Thompson, "Mr imaging of head trauma: Review of the distribution and radiopathologic features of traumatic lesions," *American Journal of Neuroradiology*, vol. 9, no. 1, pp. 101–110, 1988.

[30] K. Linka, N. Reiter, J. Würges, M. Schicht, L. Bräuer, C. J. Cyron, F. Paulsen, and S. Budday, "Unraveling the local relation between tissue composition and human brain mechanics through machine learning," *Frontiers in bioengineering and biotechnology*, vol. 9, p. 704 738, 2021.

[31] L. W. Lau, R. Cua, M. B. Keough, S. Haylock-Jacobs, and V. W. Yong, "Pathophysiology of the brain extracellular matrix: A new target for remyelination," *Nature Reviews Neuroscience*, vol. 14, no. 10, pp. 722–729, 2013.

[32] S. Budday, M Sarem, L Starck, G. Sommer, J Pfefferle, N Phunchago, E. Kuhl, F Paulsen, P Steinmann, V. Shastri, *et al.*, "Towards microstructure-informed material models for human brain tissue," *Acta Biomaterialia*, vol. 104, pp. 53–65, 2020.

[33] J. Faber, J. Hinrichsen, A. Greiner, N. Reiter, and S. Budday, "Tissue-scale biomechanical testing of brain tissue for the calibration of nonlinear material models," *Current Protocols*, vol. 2, no. 4, e381, 2022.

[34] W. L. Nowinski, "Human brain anatomy in 3d," in *Biomechanics of the Brain*, K. Miller, Ed. Cham: Springer International Publishing, 2019, pp. 5–46, ISBN: 978-3-030-04996-6. DOI: 10.1007/978-3-030-04996-6_2. [Online]. Available: https://doi.org/10.1007/978-3-030-04996-6_2.

[35] A. A. Mercadante and P. Tadi, "Neuroanatomy, gray matter," 2020.

[36] D. K. Menon, K. Schwab, D. W. Wright, A. I. Maas, *et al.*, "Position statement: Definition of traumatic brain injury," *Archives of physical medicine and rehabilitation*, vol. 91, no. 11, pp. 1637–1640, 2010.

[37] D. B. MacManus, B. Pierrat, J. G. Murphy, and M. D. Gilchrist, "Region and species dependent mechanical properties of adolescent and young adult brain tissue," *Scientific reports*, vol. 7, no. 1, pp. 1–12, 2017.

[38] D. R. Namjoshi, W. H. Cheng, A. Bashir, A. Wilkinson, S. Stukas, K. M. Martens, T. Whyte, Z. A. Abebe, K. A. McInnes, P. A. Cripton, *et al.*, "Defining the biomechanical and biological threshold of murine mild traumatic brain injury using chimera (closed head impact model of engineered rotational acceleration)," *Experimental neurology*, vol. 292, pp. 80–91, 2017.

[39] J. M. Powell, J. V. Ferraro, S. S. Dikmen, N. R. Temkin, and K. R. Bell, "Accuracy of mild traumatic brain injury diagnosis," *Archives of physical medicine and rehabilitation*, vol. 89, no. 8, pp. 1550–1555, 2008.

[40] M. Wintermark, P. C. Sanelli, Y. Anzai, A. J. Tsiouris, C. T. Whitlow, T. J. Druzgal, A. D. Gean, Y. W. Lui, A. M. Norbash, C. Raji, *et al.*, "Imaging evidence and recommendations for traumatic brain injury: Conventional neuroimaging techniques," *Journal of the American College of Radiology*, vol. 12, no. 2, e1–e14, 2015.

[41] E. D. Bigler, "Anterior and middle cranial fossa in traumatic brain injury: Relevant neuroanatomy and neuropathology in the study of neuropsychological outcome.," *Neuropsychology*, vol. 21, no. 5, p. 515, 2007.

[42] S. Kleiven, "Predictors for traumatic brain injuries evaluated through accident reconstructions," *Stapp car crash J*, vol. 51, no. 1, pp. 81–114, 2007.

[43] J Weickenmeier, C. Butler, P. Young, A. Goriely, and E Kuhl, "The mechanics of decompressive craniectomy: Personalized simulations," *Computer Methods in Applied Mechanics and Engineering*, vol. 314, pp. 180–195, 2017.

[44] S. Chatelin, A. Constantinesco, and R. Willinger, "Fifty years of brain tissue mechanical testing: From in vitro to in vivo investigations," *Biorheology*, vol. 47, no. 5-6, pp. 255–276, 2010.

[45] L. E. Bilston, "Brain tissue mechanical properties," in *Biomechanics of the Brain*, Springer, 2011, pp. 69–89.

[46] K. Miller and K. Chinzei, "Mechanical properties of brain tissue in tension," *Journal of Biomechanics*, vol. 35, pp. 483–490, 4 2002. DOI: 10.1016/s0021-9290(01)00234-2.

[47] L. A. Mihai, S. Budday, G. Holzapfel, E. Kuhl, and A. Goriely, "A family of hyperelastic models for human brain tissue," *Journal of the Mechanics and Physics of Solids*, vol. 106, pp. 60–79, 2017. DOI: 10.1016/j.jmps.2017.05.015.

[48] A. E. Forte, S. M. Gentleman, and D. Dini, "On the characterization of the heterogeneous mechanical response of human brain tissue," *Biomechanics and modeling in mechanobiology*, vol. 16, pp. 907–920, 2017.

[49] Y.-C. Fung, *Biomechanics: mechanical properties of living tissues*. Springer Science & Business Media, 2013.

[50] S. Cheng, E. C. Clarke, and L. E. Bilston, "The effects of preconditioning strain on measured tissue properties," *Journal of biomechanics*, vol. 42, no. 9, pp. 1360–1362, 2009.

[51] E. C. Ajare, F. C. Campbell, E. K. Mgbe, A. O. Efekemo, A. C. Onuh, A. Nnamani, O. Okwunodulu, and S. C. Ohaegbulam, "Mri-based morphometric analysis of corpus callosum dimensions of adults in southeast nigeria," *Libyan Journal of Medicine*, vol. 18, no. 1, p. 2 188 649, 2023.

[52] J. Hinrichsen, N. Reiter, L. Bräuer, F. Paulsen, S. Kaessmair, and S. Budday, "Inverse identification of region-specific hyperelastic material parameters for human brain tissue," *Biomechanics and Modeling in Mechanobiology*, pp. 1–21, 2023.

[53] H Bechir, A Djema, and S Bouzidi, "On poisson's functions of compressible elastomeric materials under compression tests in the framework of linear elasticity theory," *Acta Mechanica*, vol. 230, no. 7, pp. 2491–2504, 2019.

[54] O Starkova and A Aniskevich, "Poisson's ratio and the incompressibility relation for various strain measures with the example of a silica-filled sbr rubber in uniaxial tension tests," *Polymer Testing*, vol. 29, no. 3, pp. 310–318, 2010.

[55] J. Bonet and R. D. Wood, *Nonlinear continuum mechanics for finite element analysis*. Cambridge university press, 1997.

[56] R. Moran, J. H. Smith, and J. J. García, "Fitted hyperelastic parameters for human brain tissue from reported tension, compression, and shear tests," *Journal of biomechanics*, vol. 47, no. 15, pp. 3762–3766, 2014.

[57] R. H. Pritchard, P. Lava, D. Debruyne, and E. M. Terentjev, "Precise determination of the poisson ratio in soft materials with 2d digital image correlation," *Soft Matter*, vol. 9, no. 26, pp. 6037–6045, 2013.

[58] J. D. Coonrod and P. E. Dans, "Subdural empyema," *The American journal of medicine*, vol. 53, no. 1, pp. 85–91, 1972.

[59] M. Hajiaghamemar, T. Wu, M. B. Panzer, and S. S. Margulies, "Embedded axonal fiber tracts improve finite element model predictions of traumatic brain injury," *Biomechanics and modeling in mechanobiology*, vol. 19, pp. 1109–1130, 2020.

[60] C. A. Guertler, R. J. Okamoto, J. L. Schmidt, A. A. Badachhape, C. L. Johnson, and P. V. Bayly, "Mechanical properties of porcine brain tissue in vivo and ex vivo estimated by mr elastography," *Journal of Biomechanics*, vol. 69, pp. 10–18, 2018.

[61] F. Burgos-Flórez and D. A. Garzón-Alvarado, "Stress and strain propagation on infant skull from impact loads during falls: A finite element analysis," *International Biomechanics*, vol. 7, no. 1, pp. 19–34, 2020.

[62] T. W. McAllister, J. C. Ford, S. Ji, J. G. Beckwith, L. A. Flashman, K. Paulsen, and R. M. Greenwald, "Maximum principal strain and strain rate associated with concussion diagnosis correlates with changes in corpus callosum white matter indices," *Annals of biomedical engineering*, vol. 40, pp. 127–140, 2012.

[63] M. Hosseini-Farid, M. Amiri-Tehrani-Zadeh, M. Ramzanpour, M. Ziejewski, and G. Karami, "The strain rates in the brain, brainstem, dura, and skull under dynamic loadings," *Mathematical and Computational Applications*, vol. 25, no. 2, p. 21, 2020.

[64] E. Axpe, G. Orive, K. Franze, and E. A. Appel, "Towards brain-tissue-like biomaterials," *Nature Communications*, vol. 11, no. 1, p. 3423, 2020.

[65] A. Madhukar and M. Ostoja-Starzewski, "Finite element methods in human head impact simulations: A review," *Annals of biomedical engineering*, vol. 47, pp. 1832–1854, 2019.

[66] K. M. Tse, S. P. Lim, V. B. C. Tan, and H. P. Lee, "A review of head injury and finite element head models," *Am. J. Eng. Technol. Soc*, vol. 1, no. 5, pp. 28–52, 2014.

[67] A. K. Ommaya and T. Gennarelli, "Cerebral concussion and traumatic unconsciousness: Correlation of experimental and clinical observations on blunt head injuries," *Brain*, vol. 97, no. 1, pp. 633–654, 1974.

[68] M. T. Begonia, R. Prabhu, J. Liao, M. F. Horstemeyer, and L. N. Williams, "The influence of strain rate dependency on the structure–property relations of porcine brain," *Annals of biomedical engineering*, vol. 38, pp. 3043–3057, 2010.

[69] B. Rashid, M. Destrade, and M. D. Gilchrist, "Determination of friction coefficient in unconfined compression of brain tissue," *Journal of the Mechanical Behavior of Biomedical Materials*, vol. 14, pp. 163–171, 2012.

[70] B. Rashid, M. Destrade, and M. D. Gilchrist, "Inhomogeneous deformation of brain tissue during tension tests," *Computational Materials Science*, vol. 64, pp. 295–300, 2012.

[71] B. R. Donnelly and J. Medige, "Shear properties of human brain tissue," *Journal of Biomechanical Engineering*, vol. 119, pp. 423–432, 4 1997. DOI: 10.1115/1.2798289.

[72] M. T. Begonia, A. M. Knapp, R. Prabhu, J. Liao, and L. N. Williams, "Shear-deformation based continuum-damage constitutive modeling of brain tissue," *Journal of Biomechanics*, vol. 117, p. 110 260, 2021.

[73] S. Budday, R. Nay, R. De Rooij, P. Steinmann, T. Wyrobek, T. C. Ovaert, and E. Kuhl, "Mechanical properties of gray and white matter brain tissue by indentation," *Journal of the mechanical behavior of biomedical materials*, vol. 46, pp. 318–330, 2015.

[74] P. V. Bayly, E. E. Black, R. C. Pedersen, E. P. Leister, and G. M. Genin, "In vivo imaging of rapid deformation and strain in an animal model of traumatic brain injury," *Journal of biomechanics*, vol. 39, no. 6, pp. 1086–1095, 2006.

[75] J. D. Finan, S. N. Sundaresh, B. S. Elkin, G. M. McKhann II, and B. Morrison III, "Regional mechanical properties of human brain tissue for computational models of traumatic brain injury," *Acta biomaterialia*, vol. 55, pp. 333–339, 2017.

[76] L. E. Bilston, Z. Liu, and N. Phan-Thien, "Linear viscoelastic properties of bovine brain tissue in shear," *Biorheology*, vol. 34, no. 6, pp. 377–385, 1997.

[77] Y. Feng, Y. Gao, T. Wang, L. Tao, S. Qiu, and X. Zhao, "A longitudinal study of the mechanical properties of injured brain tissue in a mouse model," *Journal of the mechanical behavior of biomedical materials*, vol. 71, pp. 407–415, 2017.

[78] S Chatelin, J. Vappou, S. Roth, J.-S. Raul, and R. Willinger, "Towards child versus adult brain mechanical properties," *Journal of the mechanical behavior of biomedical materials*, vol. 6, pp. 166–173, 2012.

[79] F. Chen, J. Zhou, Y. Li, Y. Wang, L. Li, and H. Yue, "Mechanical properties of porcine brain tissue in the coronal plane: Interregional variations of the corona radiata," *Annals of biomedical engineering*, vol. 43, pp. 2903–2910, 2015.

[80] K. B. Arbogast, D. F. Meaney, and L. E. Thibault, "Biomechanical characterization of the constitutive relationship for the brainstem," SAE Technical Paper, Tech. Rep., 1995.

[81] A. Goriely, S. Budday, and E. Kuhl, "Neuromechanics: From neurons to brain," *Advances in applied mechanics*, vol. 48, pp. 79–139, 2015.

[82] K. Laksari, M. Shafieian, and K. Darvish, "Constitutive model for brain tissue under finite compression," *Journal of biomechanics*, vol. 45, no. 4, pp. 642–646, 2012.

[83] M. Takaza, K. M. Moerman, J. Gindre, G. Lyons, and C. K. Simms, "The anisotropic mechanical behaviour of passive skeletal muscle tissue subjected to large tensile strain," *Journal of the mechanical behavior of biomedical materials*, vol. 17, pp. 209–220, 2013.

[84] Y. Dong and B. Pan, "A review of speckle pattern fabrication and assessment for digital image correlation," *Experimental Mechanics*, vol. 57, pp. 1161–1181, 2017.

[85] B. Pan, "Recent progress in digital image correlation," *Experimental mechanics*, vol. 51, pp. 1223–1235, 2011.

[86] B. Pan, W. Dafang, and X. Yong, "Incremental calculation for large deformation measurement using reliability-guided digital image correlation," *Optics and Lasers in Engineering*, vol. 50, no. 4, pp. 586–592, 2012.

[87] M. T. Prange, D. F. Meaney, and S. S. Margulies, "Directional properties of gray and white brain tissue undergoing large deformation," in *ASME International Mechanical Engineering Congress and Exposition*, American Society of Mechanical Engineers, vol. 15823, 1998, pp. 151–152.

[88] (). Vic-2d, Correlated Solutions Inc., [Online]. Available: http://correlatedsolutions.com/vic-2d/.

[89] E. Jones and M. A. Iadicola, *A good practices guide for digital image correlation; international digital image correlation society, 2018*.

[90] J. Weickenmeier, R. de Rooij, S. Budday, T. C. Ovaert, and E. Kuhl, "The mechanical importance of myelination in the central nervous system," *Journal of the mechanical behavior of biomedical materials*, vol. 76, pp. 119–124, 2017.

[91] C. Stadelmann, S. Timmler, A. Barrantes-Freer, and M. Simons, "Myelin in the central nervous system: Structure, function, and pathology," *Physiological reviews*, vol. 99, no. 3, pp. 1381–1431, 2019.

[92] S. Hartmann and P. Neff, "Polyconvexity of generalized polynomial-type hyperelastic strain energy functions for near-incompressibility," *International journal of solids and structures*, vol. 40, no. 11, pp. 2767–2791, 2003.

[93] G. A. Holzapfel, *Nonlinear solid mechanics: A continuum approach for engineering science*, 2002.

[94] A. S. Shatil, M. N. Uddin, K. M. Matsuda, and C. R. Figley, "Quantitative ex vivo mri changes due to progressive formalin fixation in whole human brain specimens: Longitudinal characterization of diffusion, relaxometry, and myelin water fraction measurements at 3t," *Frontiers in medicine*, vol. 5, p. 31, 2018.

[95] J. Zhang, B. Song, F. A. Pintar, N. Yoganandan, W. Chen, and T. A. Gennarelli, "How to test brain and brain simulant at ballistic and blast strain rates," *Biomed. Sci. Instrum*, vol. 44, pp. 129–134, 2008.

[96] H. Metz, J. McElhaney, and A. K. Ommaya, "A comparison of the elasticity of live, dead, and fixed brain tissue," *Journal of Biomechanics*, vol. 3, no. 4, pp. 453–458, 1970.

[97] M. A. Sutton, J. H. Yan, V. Tiwari, H. Schreier, and J.-J. Orteu, "The effect of out-of-plane motion on 2d and 3d digital image correlation measurements," *Optics and Lasers in Engineering*, vol. 46, no. 10, pp. 746–757, 2008.

[98] B. Pan, "Bias error reduction of digital image correlation using gaussian prefiltering," *Optics and Lasers in Engineering*, vol. 51, no. 10, pp. 1161–1167, 2013.

[99] B. Pan, K. Qian, H. Xie, and A. Asundi, "Two-dimensional digital image correlation for in-plane displacement and strain measurement: A review," *Measurement science and technology*, vol. 20, no. 6, p. 062 001, 2009.

Appendix A: Digital Image Correlation (DIC) Method Summary

A summary of the Digital Image Correlation (DIC) analysis method, its parameters, and the experimental uncertainties associated with the work conducted in this thesis is presented.

A.1 Digital Image Correlation (DIC) Technique Summary

Digital Image Correlation (DIC) is an optical method that measures the full-field surface displacements and strains of a user-specified region of interest (ROI). The non-contact aspect of the technique is particularly well-suited for fragile biological tissues [22]. Its principle relies on tracking a speckle pattern on the tissue surface through successive stages of deformation. This tracking relies on an optimization algorithm that utilizes the gray levels at each image to match the corresponding subsets in the deformed state to the reference image, and thus the displacement or strain field can then be computed. VIC-2D 6 [88, 97] software, was used in this study to compute the axial and transverse strains of the mechanical tests. DIC quantifies displacements by comparing digital photographs of a specimen before and after deformation. Strains are calculated from the displacement field by differentiating displacement vectors within each subset [88].

A.2 Sample Preparation for DIC

To prepare brain tissue for testing, cylindrical samples were extracted from whole brains using a biopsy punch. These samples, measuring 6 mm in diameter, were then cut into 4 mm high segments using a scalpel and a custom-made slicing jig.

A major challenge in the DIC analysis process was applying a well-defined speckle pattern on the specimen's surface that was thin enough to not obscure the movement of the underlying surface, considering the specimen's small size. To avoid aliasing, the minimum speckle size according to literature should be 3-5 times larger than the image pixel size [89]. The camera used in this study (AOS PROMON U750 high-speed camera) has a full resolution of 1280 x 1024 pixels. Upon calibration, the image scale was found to be 0.007 mm/pixel. Therefore, the optimal speckle size was chosen to be between 21 μm to 35 μm. A random but uniform speckling is achieved by using an ultra-fine point Harder and Steenbeck Infinity airbrush with a 0.15 mm diameter needle and nozzle to apply an isopropanol-based pigment onto the samples.

A.3 Cross-Polarization Technique

In previous studies, multi-step surface treatments have been applied to limit the specular reflections caused by the hydrated brain tissues reflecting incident light back during testing such as: applying a first layer of white paint, a second layer of talcum powder to decrease the shininess of the surface, and a third layer of black speckling [14, 23]. However, that practice has many drawbacks such as adding thickness to the sample, or prematurely causing the sample to dry out due to the absorptive properties of talcum powder.

For the present study, a technique called cross-polarization was used, which consists of placing a linear polarizer in between the light source and the tested sample and another polarizer of perpendicular polarization in between the sample and the camera, as depicted first in Figure 3.2a and repeated in Figure A.1a for convenience. This

way, the specular reflections are selectively attenuated and only the diffuse non-glaring light reaches the camera, producing high-contrast images as observed in Figure A.1b and Figure A.1c and reducing the sample treatment steps required to perform DIC analysis from three [14, 23] to the single speckling step.

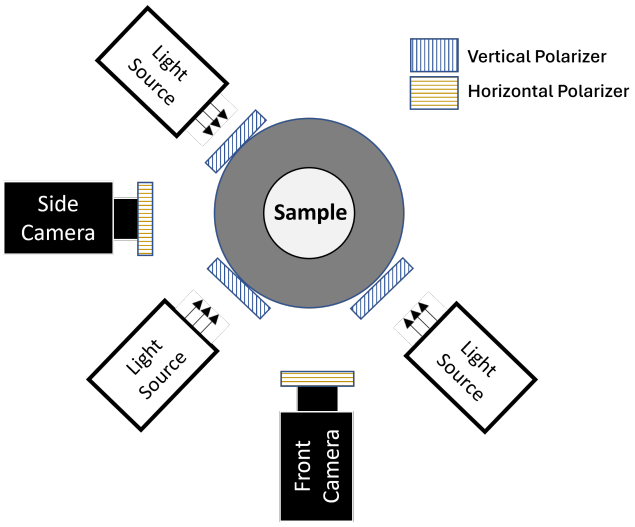

(a)

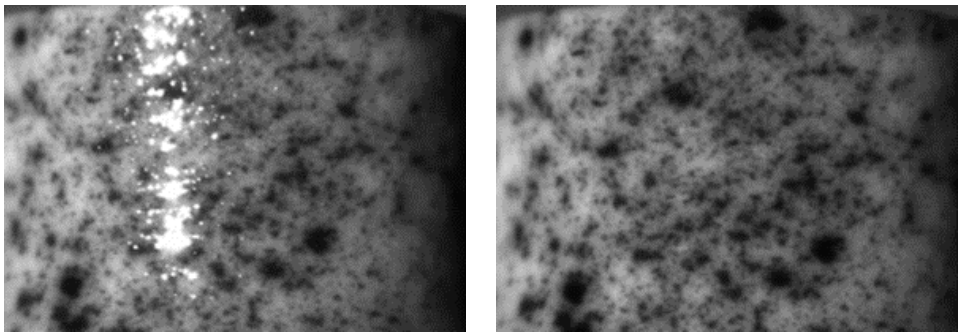

(b) (c)

Figure A.1: (a) Camera and polarizer arrangement for cross-polarization implementation for DIC, (b) hydrated tissue with no cross-polarization, and (c) same hydrated tissue captured with cross-polarization technique

A.4 Digital Image Correlation Settings

During the analysis, a Gaussian low pass filter was chosen to remove high-frequency signals and pre-smooth both the reference image (the first frame depicting the specimen's undeformed state) and the deformed images (all subsequent frames). This

pre-smoothing enhances measurement accuracy by filtering out bias signals, as noted by Pan [98].

The deformation tracking relies on an optimization algorithm that utilizes the gray levels at each image to match the corresponding subsets in the deformed state to the reference image, and thus the displacement or strain field can then be computed. A zero-normalized squared sum of difference (ZNSSD) correlation method was utilized to minimize errors caused by lighting changes or scaled discoloration of tissue. In brief, the Zero Normalized Cross-Correlation (ZNCC) criterion is a statistical measure used to assess the similarity between two images and is particularly useful for comparing subsets of an image before and after deformation [99]. The ZNCC value ranges between -1 and 1, where 1 indicates perfect correlation, 0 means no correlation, and -1 implies perfect inverse correlation [99]. This criterion is robust against both offset and scale changes in lighting intensity making it reliable for tracking displacement with minor changes in the image. It is computationally more expensive than other correlation criteria, but due to the relatively low number of images taken per test, no correlation process took longer than 3 minutes.

Incremental correlation was used for a more stable prediction in the presence of large deformations. During post-processing, rigid body motion was removed to eliminate the effect of minimal camera vibration during the experiments.

A.5 Uncertainty Quantification

The errors that can occur in DIC measurements are the variance and the bias errors. Variance errors otherwise known as noise are random errors centered about the mean true value that is being measured [89]. The noise in the measurements was minimized by using the cross-polarization technique as described in Appendix A.3, and by removing rigid body motions. Bias errors can be caused by aggressive smoothing of the data, lens distortions, and out-of-plane motions [89]. Variance errors are quantified by analyzing static images acquired before a test is performed [89]. Bias

errors, while not often possible to fully quantify, can be estimated by applying rigid body, out-of-plane translation of images. In theory, for rigid body motion, the strain measurement should be zero, meaning that any non-zero values are a combination of variance and bias errors in measurement [89].

The expected sample movement during testing is estimated to be 2 mm. Therefore, to estimate the error due to out-of-plane, the sample was moved 2 mm away and toward the camera at 20 mm/s, which is the same displacement rate applied to the samples in the study during the high-rate compression tests. The same capturing parameters as in actual tests were used. The uncertainty due to variance and bias for the tests performed in the present study are shown in Figure A.2. The deviation from the true value of $stretch = 1$ due to variance (noise) can be observed by the static images starting from Image index 0 to 30 and is shown to be less than 0.0005, while the uncertainty due to out-of-plane motion seen in Image index 35 - 59 show maximum values of 0.0032. These values are small compared to the strains of 0.7, which provides reassurance in the measurements obtained.

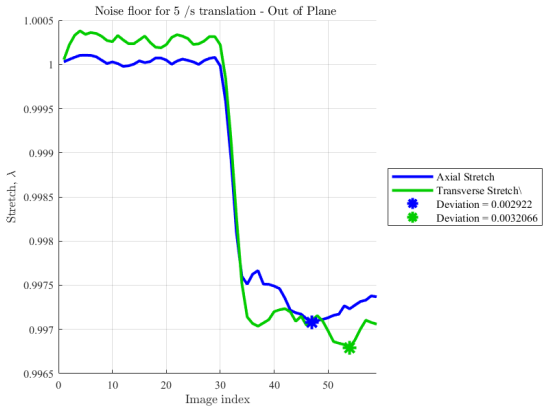

Figure A.2: Estimation of measurement uncertainty

Appendix B: MATLAB Scripts

The data analysis in the presented work was primarily conducted using MATLAB. This appendix contains the relevant scripts used for data importation, filtering, conversion from strain to stretch, matching DIC to compression data, and calculation of parameters such as stress, Poisson Function, and volume ratio.

B.1 DIC Data Read and Conversion

Listing B.1: Analysis of output DIC data from VIC-2D software

```
%======= Description ==========
% This function takes in the raw data from DIC and outputs the time steps and
    stretches (axial and transverse) according to the specified frame rate during
    capture.
%------ Inputs -------
% DIC_Folder: Where VIC-2D output files (in.csv format) are located
% Rate: '0p05' or '5ps' corresponding to 0.05 /s and 5 /s strain rates
% Region: TL (Temporal Lobe), CCwF (Corpus Callosum compressed along its fiber
    direction), CCxF (Corpus Callosum Compressed across
% its fiber direction
% fps: 30 fps for slow strain rate, 309 fps for faster strain rate
% view: Either Front or Left. Corresponding to the cameras used. The front camera
    always was set to record along the fiber
% direction of samples in CCxF tests
%------ Outputs --------
% t_DICs: Time steps as calculated by fps. Each time step is 1/fps long
% stretches_x_DIC & stretches_y_DIC: Stretches as obtained from Lagrange strain
    definition sqrt(2.*strains_Lagrange+1);
%======= End of Description ========
%-----------------------------------------
% For DIC
%-----------------------------------------
    fps=309;
    directory =DIC_Folder;
    switch rate
       case '0p05'
          fps=30;
    end
cd(directory);
% Extract file indices of tests of interest
fileList = dir('*.csv');
region_index = contains({fileList.name}, region);
rate_index = contains({fileList.name}, rate);
view_index = contains({fileList.name}, view);
test_index = find(region_index & rate_index & view_index);

```

```
% Do a for loop to go though all the iterations
for ii = 1:length(test_index)
        % Extracting data from .csv files
        iii=test_index(ii);
        exp_name_DIC = fileList(iii).name;
        [NoOfRows,NoOfColumn] = size(readmatrix(exp_name_DIC));
        opts = delimitedTextImportOptions("NumVariables", NoOfColumn);
        opts.DataLines = [3, NoOfRows];
        opts.Delimiter = ",";
        opts.VariableTypes = repmat({'double'}, 1, NoOfColumn);
        opts.VariableNamesLine = 2;
        opts.ExtraColumnsRule = "ignore";
        opts.EmptyLineRule = "read";
        opts.VariableNames = {'Index','x_pixel','y_pixel','X_pixel','Y_pixel','
            u_pixel','v_pixel','U _pixel','V_pixel','exx_1__Lagrange','
            eyy_1__Lagrange','exy _1__Lagrange', 'e1_Lagrange','e2_Lagrange','
            gamma_Lagrange'};
        exp_DIC = readtable(exp_name_DIC,opts);

        % Time and stretch for DIC
        t_DIC = exp_DIC.Index.*(1/fps);
        % ------- Smoothing of strain data
        n = length(t_DIC);
        average_no=floor((n/40)+1); % Adjust this based on data length
        strains_y_G = exp_DIC.eyy_1__Lagrange;
        strains_x_G = exp_DIC.exx_1__Lagrange;
        % Conversion to stretch
        stretch_y_DIC = smoothdata(sqrt(2.*strains_y_G+1),'sgolay',average_no);
        stretch_x_DIC = smoothdata(sqrt(2.*strains_x_G+1),'sgolay',average_no);

       % Removing data before initial displacement
        idx = find(stretch_y_DIC<0.995,1,"first");
        if idx==1
            idx=2;
        end
        t_DIC = t_DIC - t_DIC(idx-1);
        t_DIC(1:idx-2) = [];
        stretch_y_DIC=stretch_y_DIC-stretch_y_DIC(idx-1)+1;
        stretch_x_DIC=stretch_x_DIC-stretch_x_DIC(idx-1)+1;
        stretch_y_DIC(1:idx-2) = [];
        stretch_x_DIC(1:idx-2) = [];

        % Slope calculation
        strain_rate = diff(stretch_y_DIC)./diff(t_DIC);

        % Removing data to avoid repeating values
        switch rate
            case '0p05'
                idy = find(strain_rate<-0.04,1,"last")+1;
          case '5ps'
                idy = find(strain_rate<-3,1,"last")+1;
        end

        t_DIC(idy+1:end) = [];
        stretch_y_DIC(idy+1:end)=[];
        stretch_x_DIC(idy+1:end)=[];

        %Storing values
        stretches_x_DIC{ii}=stretch_x_DIC;
        stretches_y_DIC{ii}=stretch_y_DIC;
        t_DICs{ii} = t_DIC;
end
```

B.2 Mach-1 Data Read and Conversion

This function takes in the raw data from Mach-1 and outputs the time steps, and converts displacement and force to stretch and stresses, respectively.

Listing B.2: Analysis of output compression test data from Mach-1

```
%% Mach1 Data Collection and Analysis
% ======= Description ==========
%This function takes in the raw data from Mach-1 and outputs the time steps, and converts disp and force to stretch and stresses.
% ----- Inputs ------
% Mach1_Folder: Where output files (in .txt format) are located
% Rate: '0p05' or '5ps' corresponding to 0.05 /s and 5 /s strain rates
% Region: TL (Temporal Lobe), CCwF (Corpus Callosum compressed along its fiber direction), CCxF (Corpus Callosum Compressed across
% its fiber direction
% ------ Outputs --------
% ts: Time steps along test
% stretches: Stretches as obtained from Lagrange strain definition sqrt(2.*strains_Lagrange+1);
% stresses: Stresses were computed by F/A where F is the reaction force during test and A is the original cross sectional area of sample

cd(Mach1_Folder);
fileList = dir('*.txt');
region_index = contains({fileList.name}, region);
rate_index = contains({fileList.name}, rate);
test_index = find(region_index & rate_index);

for ii = 1:length(test_index)
        iii=test_index(ii);
        exp_name_Mach = fileList(iii).name; % <------ Change number to change experiment
        opts = delimitedTextImportOptions("NumVariables", 10);
        n = linecount(exp_name_Mach);
        opts.DataLines = [26, n-3];
        opts.Delimiter = "\t";
        opts.VariableNames = ["t", "z", "x", "y", "FxN", "FyN", "FzN", "TxNmm", "TyNmm", "TzNmm"];
        opts.VariableTypes = ["double", "double", "double", "double", "double", "double", "double", "double", "double", "double"];
        opts.ExtraColumnsRule = "ignore";
        opts.EmptyLineRule = "read";
        exp_Mach = readtable(exp_name_Mach,opts);

% Cross Sectional Area
        CSA = (pi()*0.006^2)/4; %[m^2]



% Original time, disp, force, stress
        t = exp_Mach.t;
        stretch = abs(exp_Mach.z./exp_Mach.z(1));
        force = abs(exp_Mach.FzN);
% Define filter parameters
        average_no=floor((n)/100); % Adjusted window length based on data length, n
% Apply low pass filter and smooth data
        LPassedData = lowpass(force,120,1/t(2));
        smoothedForce= smoothdata(LPassedData,'sgolay',average_no);
        stress = smoothedForce./CSA;


```

```
% Removing data before initial displacement for Mach1
        idxx = find(stretch<0.999, 1, 'first');
        t = t - t(idxx-1);
        t(1:idxx-2) = [];
        stress=stress-stress(idxx-1);
        stretch=stretch-stretch(idxx-1)+1;
        stretch(1:idxx-2) = [];
        stress(1:idxx-2) = [];

% Removing data after stretch to avoid repeated values
        idy = find(stretch<0.65,1,"first");
        t(idy+1:end) = [];
        stretch(idy+1:end)=[];
        stress(idy+1:end)=[];

% Storing values of each iteration
        stretches{ii}=stretch;
        stresses{ii}=stress;
        ts{ii}=t;
end
```

B.3 Incorporating Optical and Mechanical Data

Listing B.3: Matching strain from DIC to Mach expressed in terms of stretches

```
% ====== DESCRIPTION ==============
% Matching DIC and Mach-1 stretch values
% Takes Brain Number (brain_no), strain rate (0p05, 5ps), and region (TL, CCxF,CCwF)
    and summarizes data from Mach1 and DIC
% Outputs TLDR(:,:,views) = [stretches_y_DIC, poissons_G, stress_interp4DICs,
    stretches_Mach1s,stretches_x_DIC,t_DICs];

for views = 1:2;

% Rate and Region
    vieww = {'Front','Left'};
    view = vieww{views};
%---------------------------------------
% DIC data
%---------------------------------------
    % fps change depending on strain rate
    switch rate
       case '0p05'
          fps=30;
      case '5ps'
          fps=309;
    end

    directory =DIC_Folder;
    [t_DICs,stretches_x_DIC,stretches_y_DIC] = DICsummary4(directory,rate,region,fps,
        view);

%-------------------------
% Mach-1 data
%-------------------------
    directory=Mach1_Folder;
    [ts,stretches,stresses] = Mach1summary_stretches4(directory,rate,region);

%-----------------------------------------------
% Resample stress to match with DIC
%-----------------------------------------------
    method = 'pchip';
    % Why pchip? Because this interpolation scheme doesn't overshoot data if not
        smooth,
    % especially useful if the data is monotonic (not oscillatory)
    for i = 1:size(ts,2)
        % Actual interpolation
        % Interp1 returns values of stretches at query points t_DICs as obtained by
            interpolation
        stretches_Mach1 = interp1(ts{i}, stretches{i}, t_DICs{i},method);
        stress_interp4DIC = interp1(ts{i}, stresses{i}, t_DICs{i},method);
        stretches_Mach1s{i} = stretches_Mach1;
        stress_interp4DICs{i} = stress_interp4DIC./1000; % Convert to kPa
    end

for iii = 1:size(ts,2)
        poisson_G = (1-stretches_x_DIC{iii}.^2)./(stretches_y_DIC{iii}.^2-1);
        poissons_G{iii} = poisson_G;
end

% Output Data
TLDR(:,:,views) = [stretches_y_DIC, poissons_G, stress_interp4DICs,stretches_Mach1s,
    stretches_x_DIC,t_DICs];
end
```

B.4 Computing Volume Ratio, J

Listing B.4: Computing volume ratio

```
function [TLDR1 TLDR2] = JStretch4(brain,rate,region)

[TLDR1] = CompressionSummary4(brain,rate,region);

% Loading the TLDR variable for all rates/regions and changing name accordingly
CCxF_0p05_Front = TLDR1(:,:,1); % Front camera data
CCxF_0p05_Left = TLDR1(:,:,2); % Side camera data
iter = size(TLDR1,2)./6; % We have 6 different parameters in TLDR so dividing by 6
    will give us number of tests done per test type

for i = 1:iter
% Averaging the stretch measurement from both cameras in the axial direction
CCxF_0p05_stretches_11 = CCxF_0p05_Front{i};
CCxF_0p05_stretches_12 = CCxF_0p05_Left{i};
minlen = min(length(CCxF_0p05_stretches_12),length(CCxF_0p05_stretches_11));
% Obtaining the stretches in 3 directions
CCxF_0p05_stretches_1 = (CCxF_0p05_stretches_11(1:minlen)+CCxF_0p05_stretches_12(1:
    minlen))./2;
CCxF_0p05_stretches_2 = CCxF_0p05_Front{4.*iter+i};
CCxF_0p05_stretches_3 = CCxF_0p05_Left{4.*iter+i};
CCxF_0p05_stresses = CCxF_0p05_Left{2.*iter+i};
minlen = min([length(CCxF_0p05_stretches_1),length(CCxF_0p05_stretches_2),length(
    CCxF_0p05_stretches_3)]);
% Computing J by multiplying stretches in 3 directions as shown in Equation (3.3)
J = CCxF_0p05_stretches_11(1:minlen).*CCxF_0p05_stretches_2(1:minlen).*
    CCxF_0p05_stretches_3(1:minlen);
% Storing J and stretch results from all iterations
JCatch{i} = J;
Stretch1Catch{i} = CCxF_0p05_stretches_1(1:minlen);
end

% Output Data
TLDR2 = [Stretch1Catch,  JCatch];
end
```